Geochemistry Geophysics Geosystems G3

Article
Volume 13, Number 4
28 April 2012
Q04012, doi:10.1029/2011GC003987
ISSN: 1525-2027

Published by AGU and the Geochemical Society

Morphology of the Faial Island shelf (Azores): The interplay between volcanic, erosional, depositional, tectonic and mass-wasting processes

R. Quartau
Unidade de Geologia Marinha, Laboratório Nacional de Energia e Geologia I.P., Estrada da Portela-Zambujal, 2721-866 Alfragide, Portugal (rui.quartau@lneg.pt)

F. Tempera
Departamento de Oceanografia e Pescas, Universidade dos Açores, Cais de Santa Cruz, 9901-862 Horta, Açores, Portugal (tempera@uac.pt)

N. C. Mitchell
School of Earth, Atmospheric and Environmental Sciences, University of Manchester, Williamson Building, Oxford Road, Manchester M13 9PL, UK (neil.mitchell@manchester.ac.uk)

L. M. Pinheiro
Departamento de Geociências and CESAM, Universidade de Aveiro, 3810-193 Aveiro, Portugal (lmp@ua.pt)

H. Duarte
Unidade de Geologia Marinha, Laboratório Nacional de Energia e Geologia I.P., Estrada da Portela-Zambujal, 2721-866 Alfragide, Portugal

P. O. Brito
Unidade de Geologia Marinha, Laboratório Nacional de Energia e Geologia I.P., Estrada da Portela-Zambujal, 2721-866 Alfragide, Portugal

CIMAR Associate Laboratory, 2721-866 Alfragide, Portugal

C. R. Bates
School of Geography and Geosciences, University of St. Andrews, Irvine Building, North Street, St Andrews, Fife KY16 9AL, Scotland, UK (crb@st-andrews.ac.uk)

J. H. Monteiro
Unidade de Geologia Marinha, Laboratório Nacional de Energia e Geologia I.P., Estrada da Portela-Zambujal, 2721-866 Alfragide, Portugal

[1] The extents of volcanic island shelves result from surf erosion, which enlarges them, and volcanic progradation, which reduces them. However, mass-wasting, tectonics and sediment deposition also contribute to their morphology. In order to assess the relative significance of these various processes, we have mapped in detail Faial Island's shelf in the Azores archipelago based on interpretation of geophysical and geological data. The nearshore substrates of the island, down to 30–50 m depth, are rocky and covered by volcaniclastic boulder deposits formed by surf action on now-submerged lava flows. Below those depths, sandy and gravel volcaniclastic beds dominate, building clinoforms up to the shelf edge. In some sectors of the coast,

prograding lava has narrowed the shelf, but, in contrast to nearby Pico Island, we find fewer submarine-emplaced lavas on the shelf. In this island, we interpret the distance between the coastline and the shelf edge as almost entirely a result of a straightforward competition between surf erosion and lava progradation, in which erosion dominates. Therefore shelf width can be used as a proxy for coastline age as well as for wave energy exposure. The stratigraphy of shelf deposits in boomer seismic data is examined in detail to assess the roles of different sediment sources, accommodation space and wave exposure in creating these deposits. We also show evidence of mass-wasting at the shelf edge and discuss the possible origins of slope instability. Finally, we discuss the contributing role of tectonics for the development of the shelf.

Components: 14,700 words, 16 figures, 4 tables.

Keywords: coastal erosion; lava progradation; model; shelf development; shelf stratigraphy; volcanic ocean island.

Index Terms: 3022 Marine Geology and Geophysics: Marine sediments: processes and transport; 3045 Marine Geology and Geophysics: Seafloor morphology, geology, and geophysics; 3070 Marine Geology and Geophysics: Submarine landslides.

Received 30 November 2011; **Revised** 5 March 2012; **Accepted** 9 March 2012; **Published** 28 April 2012.

Quartau, R., F. Tempera, N. C. Mitchell, L. M. Pinheiro, H. Duarte, P. O. Brito, C. R. Bates, and J. H. Monteiro (2012), Morphology of the Faial Island shelf (Azores): The interplay between volcanic, erosional, depositional, tectonic and mass-wasting processes, *Geochem. Geophys. Geosyst.*, *13*, Q04012, doi:10.1029/2011GC003987.

1. Introduction

[2] Although there has been considerable interest in the geological structures and evolutions of volcanic islands [*Carracedo*, 1999; *Collier and Watts*, 2001; *Favalli et al.*, 2005; *Garcia and Davis*, 2001; *Masson et al.*, 2008; *McMurtry et al.*, 2004; *Menard*, 1984; *Mitchell*, 2003; *Mitchell et al.*, 2002; *Moore et al.*, 1994; *Oehler et al.*, 2008; *Paduan et al.*, 2009; *Quidelleur et al.*, 2008; *Ramalho et al.*, 2010b; *Schmincke*, 2004; *Scott and Rotondo*, 1983; *Staudigel and Clague*, 2010; *Wolfe et al.*, 1994] little attention has been paid to the insular shelves of such islands. Based on relatively limited data on their structures, *Menard* [1983, 1986] made some basic observations, such as how their morphologies relate to wind directions (erosion by surf) and suggested that their extents mainly reflect a competition between processes that enlarge them (e.g., principally coastline retreat by surf erosion) and processes that fill in the shelf bathymetry (e.g., volcanism and sediment deposition). Since then, only a limited number of studies have looked at the processes acting on island shelves [*Chiocci and Romagnoli*, 2004; *Coulbourn et al.*, 1974; *Grossman et al.*, 2006; *Hampton et al.*, 2004; *Mattox and Manga*, 1997; *Mitchell et al.*, 2008; *Moore et al.*, 1973; *Morelock et al.*, 1983; *Schneidermann et al.*, 1976]. However, there has remained a lack of detailed data to allow a comprehensive assessment of the processes involved in their development. *Quartau et al.* [2010] extended those efforts by comparing the morphology of the present-day Faial island shelf with a synthetic profile predicted by numerical modeling to assess the role of surf erosion in shelf widening. The model involved horizontal erosion by wave force that varied according to how sea level has fluctuated through the Quaternary. Discrepancies between the simulated and observed morphology highlighted areas where factors other than surf erosion were probably involved (i.e., processes not included in the model). Although, a variety of processes were suggested to explain the differences found, their roles were not fully understood. In this paper, we describe in more detail the morphology of Faial's shelf and interpret from the observations the roles of volcanism, seismicity, waves, climate, tectonics, types and sediment supply in shaping its morphology. We also link the onshore and offshore geology of the island. Finally, we propose a conceptual model of shelf development that can be applied to oceanic volcanic islands where wave erosion and volcanic progradation are the main processes in determining shelf morphology.

2. Regional Setting

[3] The Azores archipelago is located in the central North Atlantic Ocean and is the result of the volcanic activity around the triple junction between the American, Eurasian and African lithospheric plates (Figure 1). Nine main islands are distributed over the Azores Volcanic Plateau. The western group of

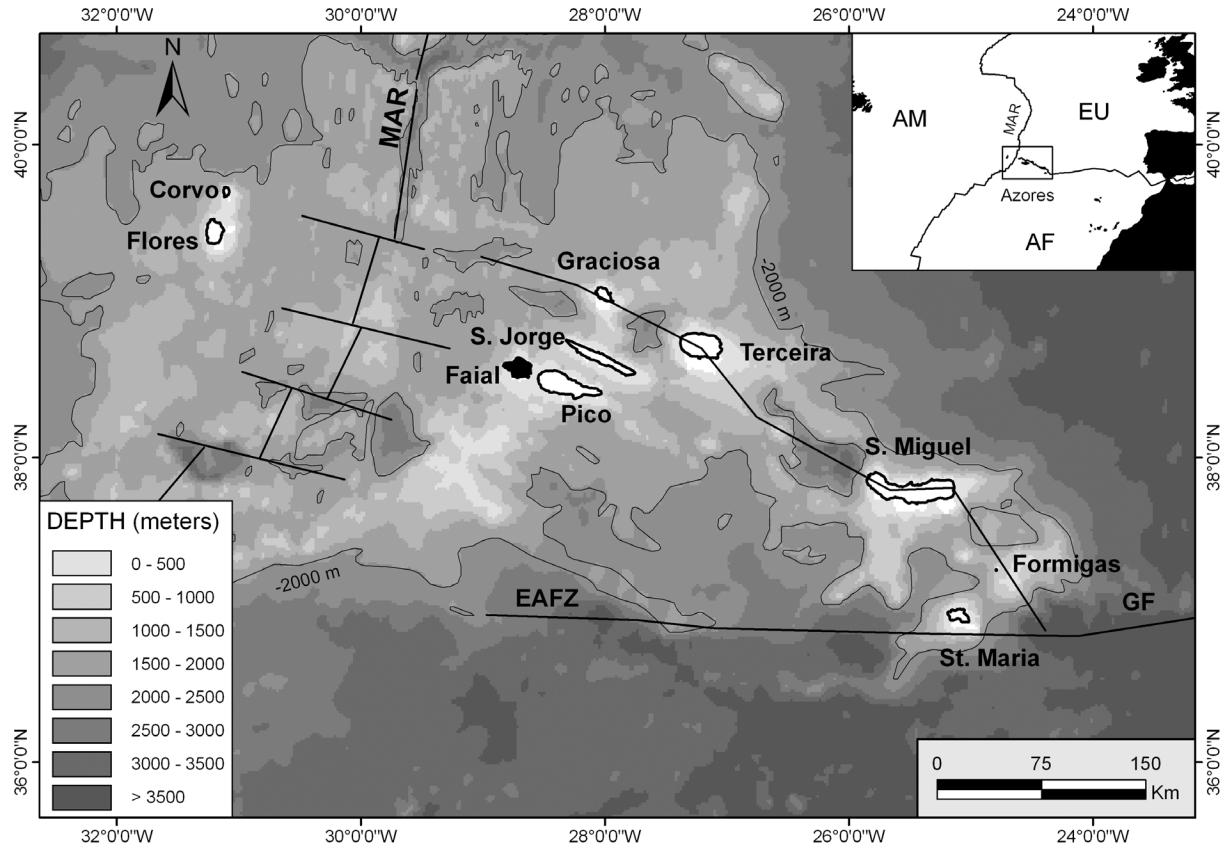

Figure 1. The Azores Archipelago, showing its relationship to the Mid-Atlantic Ridge (MAR), the American (AM), Eurasian (EU) and African (AF) plates, the East Azores Fracture Zone (EAFZ) and the Gloria Fault (GF). Faial Island is highlighted in black. Bathymetry of the Azores archipelago from the *Intergovernmental Oceanographic Commission et al.* [2003].

islands is separated from the central and eastern groups by the Mid-Atlantic Ridge, which separates the American from the Eurasian and African plates. To the east of the ridge, the East Azores fracture Zone (EAFZ) marks the boundary between Eurasia and Africa [*Krause and Watkins*, 1970; *Laughton and Whitmarsh*, 1974]. The central and eastern group are located on a wide transtensional region, result of the oblique separation across the Eurasian–African plate boundary passing through the Azores [*Lourenço et al.*, 1998]. Faial Island belongs to the central group and is the subaerial expression, together with Pico Island, of a major WNW-ESE ridge that extends over 100 km and rises from a depth of 1200–1600 m.

2.1. Geological Setting

[4] Faial Island can be subdivided into the following four morphologic regions (upper left inset in Figure 2a), which roughly correspond to the four main volcanic-stratigraphic units [*Madeira*, 1998; *Madeira and Brum da Silveira*, 2003].

[5] The Pedro Miguel Graben develops on northeast Faial where the oldest volcanic structure of the island, the Ribeirinha shield volcano, is located (Figures 2a and 2b). It is predominantly composed of subaerial hawaiitic lava flows of the Ribeirinha Volcanic Complex (800–580 ka [*Féraud et al.*, 1980]) and it is crossed by WNW-ESE trending graben (Figures 2a and 2c). The drainage pattern is deviated by the major fault scarps onto the east (Figure 2c).

[6] Over the western part of Ribeirinha volcano developed the Caldeira Volcano (Figures 2a and 2b), a stratovolcano that dominates the center of the island and constitutes its main relief, reaching 1043 m above sea level. It has a 15 km diameter at sea level and a summit truncated by a 2 km wide caldera. It is divided into two volcanostatrigraphic units. The lower unit, the Cedros Volcanic

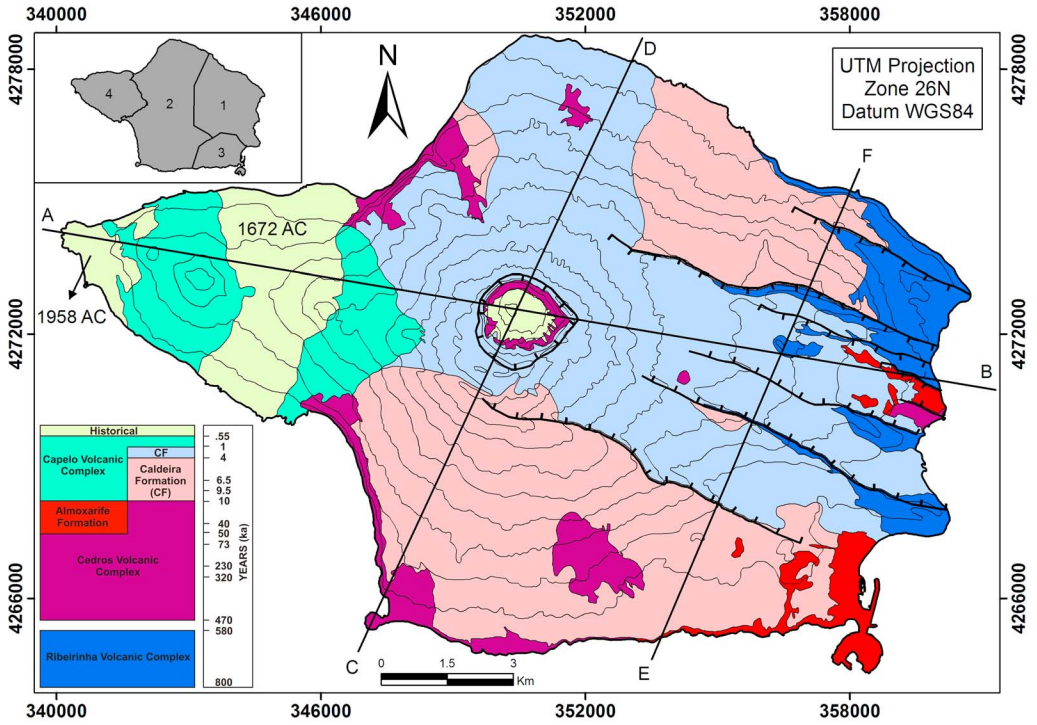

Figure 2a. Simplified geologic map and stratigraphic column of Faial Island (modified after *Madeira* [1998] and *Madeira and Brum da Silveira* [2003]). Upper left inset map locates the morphologic regions (1- Pedro Miguel Graben, 2- Caldeira Volcano, 3- Horta-Flamengos-Feteira 4- Capelo Peninsula) as defined by *Madeira* [1998]. Black straight lines orient the geological profiles shown in Figure 2b. Bold black lines with tick marks represent normal faults. Continuous topography contours are shown spaced every 100 m.

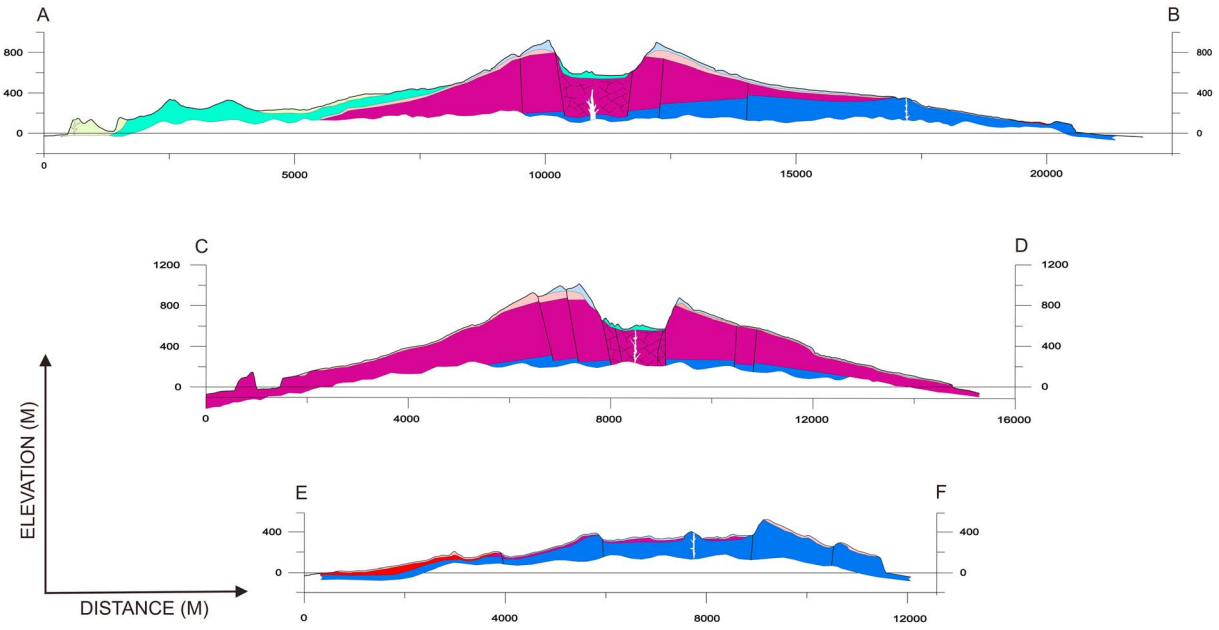

Figure 2b. Geological profiles of Faial Island (modified after *Madeira and Brum da Silveira* [2003] and *Serralheiro et al.* [1989]). Profile locations are in Figure 2a.

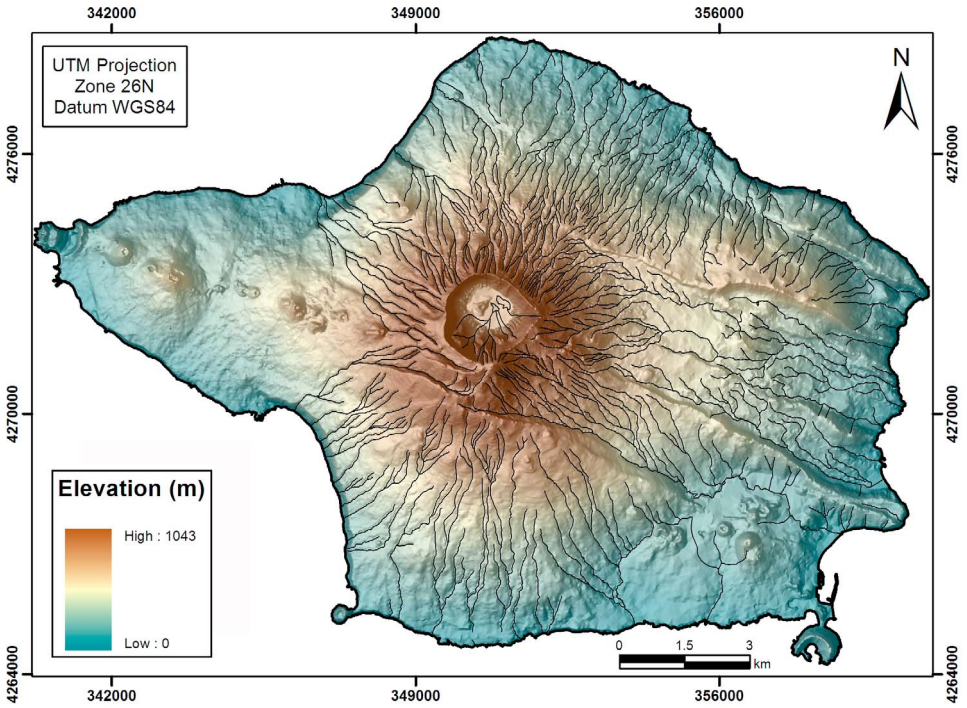

Figure 2c. Subaerial morphology and hydrographic network, based on the *Instituto Geográfico do Exército* [2001a, 2001b, 2001c, 2001d] topographic maps.

Complex, is mainly composed of subaerial basalt to benmoreite lava flows, some scoria cones and trachytic domes. According to *Féraud et al.* [1980] and *Chovelon* [1982] this unit ranges from 470 ka to 11 ka. The upper unit, the Caldeira Formation, corresponds to a sequence of trachyte pumice fall deposits, phreatic and phreatomagmatic breccias, surges, ignimbrites and lahars, emplaced by explosive eruptions (of sub-plinian style from the formation of the summit caldera). Radiocarbon dating revealed ages that range from 10 ka to 1 ka [*Madeira et al.*, 1995]. A more up-to-date stratigraphic assessment however, revealed ages ranging from 16 ka to the Present [*Pacheco*, 2001]. At its surface, the Caldeira Volcano is almost completely covered by the Caldeira Formation whose thickness can reach dozens of meters in the upper caldera slopes, diminishing toward the littoral zone (Figure 2b). Above this formation, a radial stream drainage has developed (Figure 2c) eroding the superficial pyroclastic deposits and exposing the lava flows of Cedros Volcanic Complex beneath. The WNW-ESE trending graben extends well into the Caldeira Volcano region, partially obscured in the west by the deposits of the Caldeira Formation.

[7] The Horta-Flamengos-Feteira region is characterized by a set of scoria cones and lava flows from a basaltic fissural unit (Almoxarife Formation, Figure 2a) that overlie the southeastern slope of the Caldeira volcano and the southern part of the Ribeirinha Volcano (Figure 2b). The Almoxarife Formation was dated as 30 ± 20 ka (K/Ar [*Féraud et al.*, 1980]), although its offshore part was probably formed by erosion of the flanks of Ribeirinha volcano and therefore the region where the Almoxarife Formation lies is 800 ka in age [*Quartau et al.*, 2010]. Almost this entire region and the western part of Pedro Miguel Graben are covered by a thin blanket of pyroclasts from the Caldeira Formation. The drainage network in the Horta-Flamengos-Feteira region is incipient (Figure 2c).

[8] The Capelo Peninsula, in the far west of Faial, comprises a dextral *en échelon* alignment (WNW-ESE) of basaltic Hawaiian/Strombolian cones and associated lava flows of the Capelo Volcanic Complex (Figures 2a and 2c). The eastern half of the peninsula is built on the west subaerial slope of the Caldeira volcano and overlies the oldest pyroclastic rocks of the Caldeira Formation, suggesting an age of less than 16 ka. The peninsula has been affected by two historical eruptions (1672 and 1958

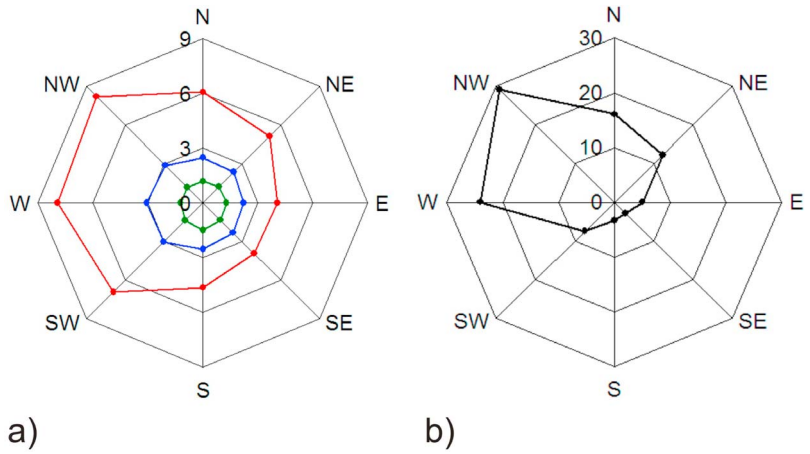

Figure 3. Faial wave dominant regimes (adapted from *Carvalho* [2002]). (a) Annual maximum (red), medium (blue) and minimum (green) significant wave height (Hs) in meters. (b) Annual frequency of the waves in percentage.

AC marked in Figure 2a), since the islands where colonized in the 15th century. The 1672 AC eruption included Strombolian activity, which formed cinder cones and erupted lava, which flowed from the vents on the rift zone both to the north and south and entered the sea. Capelinhos formed in 1958 at the most westerly tip of the island, in a classic surtseyan eruption [*Cole et al.*, 1996, 2001]. Due to its youth, the Capelo Peninsula does not have a drainage network (Figure 2c).

[9] Faial's lack of wide-valleys and sharp ridges seen in some other volcanic islands demonstrate its young geomorphology and relative lack of subaerial erosion. Even the oldest regions (central and northeast), are mostly covered by the recent pyroclasts of the Caldeira Formation and stream drainage is not significantly incised (just a few meters typically) on the lava pile beneath the pyroclastic sequence. These streams are ephemeral and most of them end at suspended valleys on the littoral cliffs. Steep cliffs dominate the coastline of Faial with sharp angles at their bases and a common small accumulation of rounded boulders in the intertidal zone. This coastal morphology suggests that wave erosion is the most important process in controlling the position of the coastline [*Borges*, 2003; *Quartau*, 2007; *Quartau et al.*, 2010].

2.2. Climate

[10] The Azores archipelago is located in the Northern Hemisphere subtropical anticyclone zone, directly under the seasonal Azores anticyclone. From September to March, the polar-front jet often migrates to the south and the Azores region is affected by low-pressure systems causing stormy weather and intermittent strong winds. It is during this season that three quarters of the total annual precipitation occurs. During late spring and summer, the Azores climate is influenced by the Azores anticyclone and there is less rain [*Ferreira*, 1981; *Santos et al.*, 2004]. However, during the Atlantic hurricane season (summer and autumn) several hurricanes can reach the Azores archipelago. Although often downgraded to tropical cyclones or depressions, they still produce heavy rain and strong winds [*Andrade et al.*, 2008]. Otherwise, the islands are characterized by an oceanic temperate climate, with mild temperatures all year-round, at low altitudes, and a rather wet climate. The distribution of rainfall is highly influenced by topography, which controls the wind speed and direction and forces the ascent of moist air, generating orographic rainfall at high altitudes. Therefore, Faial shows a typical circular precipitation pattern related to altitude, with annual precipitation ranging from 600 mm at sea level to 2800 mm in the central caldera [*Forjaz*, 2004].

2.3. Oceanographic Setting

[11] The Azores archipelago is subjected to small semidiurnal tides, with an annual mean range at Faial Island of 0.9 m [*Instituto Hidrográfico*, 2000]. Information regarding wave conditions is based on *Carvalho*'s [2002] hindcast data. The annual prevailing waves (Figure 3) are from the NW (29%) and W (24%). They are also the highest, with average significant wave height (H_s) of 2.9 m and 3.1 m respectively. Waves from the N are also important (16%) with H_s of 2.5 m. Less frequent (8%), but with high H_s (3.1 m) are waves from the SW. Records show that the Azores are struck, on average, every seven years by violent storms

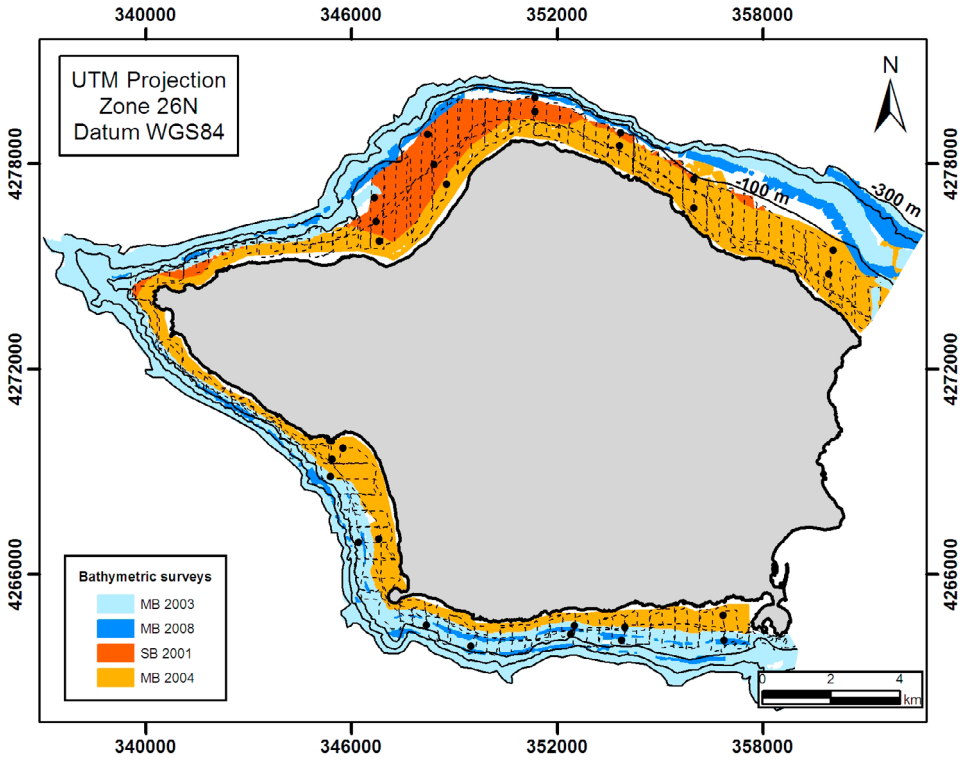

Figure 4. Location of the surveys. The bathymetry contours are depicted with solid lines and the boomer, chirp and single-beam echo-sounding survey tracks with dashed lines. Colors mark the different bathymetric data sets listed in the key (lower-left). Black dots represent sediment sampling locations.

[*Andrade et al.*, 2008], associated with remarkable wave energy. For instance, the instrumentally recorded storm of 26–27 February 2005 in Terceira Island produced H_s exceeding 5 m for a period of 19 h, with a maximum H_s of 7.66 m and a recorded maximum wave height of 15.09 m [*Instituto Hidrográfico*, 2005].

3. Material and Methods

3.1. Seismic Surveys

[12] High resolution seismic reflection profiles were collected with a chirp sonar system (Datasonics CAP-6000W) and a boomer (EG&G 230–1) in July 2001, on R/L Águas Vivas around Faial Island [*Quartau et al.*, 2002; *Teixeira*, 2001]. The chirp signal bandwidth was 1.5–10 kHz, output power 1 kW, and chirp length 10 ms (approx. vertical resolution of 10–15 cm). The boomer output energy used was 200 J, and the receiver array consisted of a single-channel streamer with 24 hydrophones. The signal frequency bandwidth ranged 250 to 1000 Hz (estimated vertical resolution < 2 m). Our seismic track planning was optimized for aggregate mapping purposes and so unfortunately the seismic data do not generally extend to the shelf edge. Nevertheless, a total of 500 km of seismic lines where acquired between 10 and 100 m water depth, 275 km of chirp and 225 km of boomer (Figure 4). Survey lines were mainly normal to the shore. An additional line was run around the island, parallel to the coastline, crosscutting the shore-normal lines at approximately 40 m water depth.

[13] The boomer seismic data was processed using the Seismic Processing Workshop software (Parallel Geoscience Corp., version 1.8.19). The processing flow included a frequency bandpass filter for noise suppression, normal moveout correction for improved accuracy on estimating reflector depths and a three trace mix for better signal-to-noise ratio. After processing, the profiles were imported for interpretation into Geology & Geophysics software applications from Landmark Graphics Corp. Most of the sub-bottom analysis was carried out on the boomer data, whereas the chirp was used for seabed classification, which confirmed the presence of sand or gravel because of lack of penetration. Electrical noise degraded the signal-to-noise ratio in some profiles, resulting in some unmapped areas.

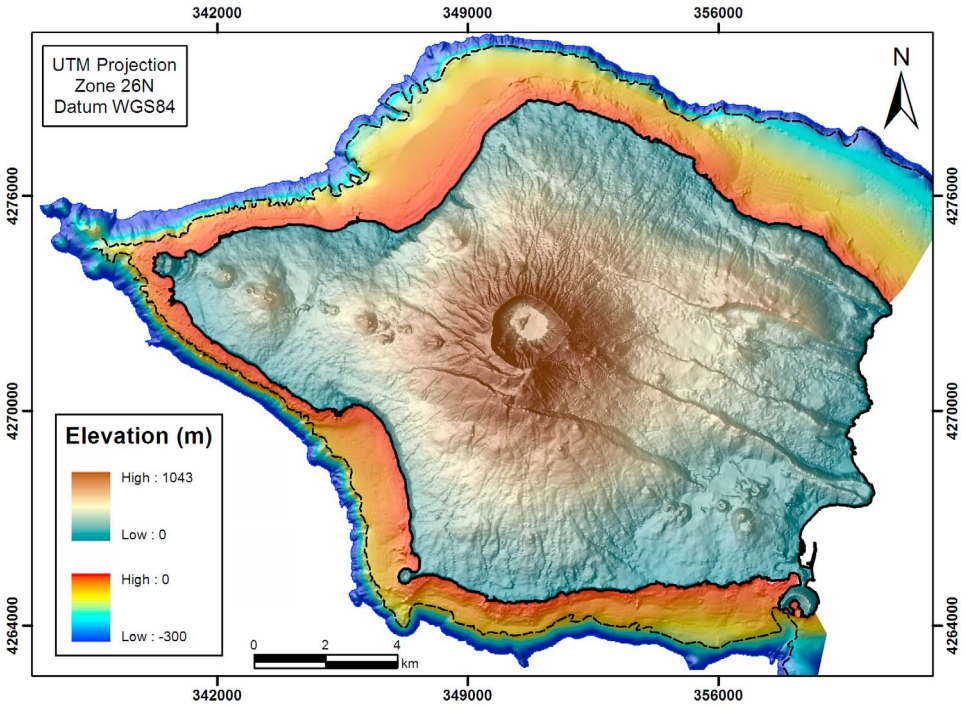

Figure 5. Offshore: shaded relief imagery derived from the bathymetric compilation. Black line depicts the coastline and dashed line the shelf edge. Onshore: DEM based on the *Instituto Geográfico do Exército* [2001a, 2001b, 2001c, 2001d] topographic maps.

3.2. Bathymetric Data

[14] High-resolution bathymetry of the outer shelf and slope of the Faial Island [*Mitchell et al.*, 2008, 2003b] was acquired in 2003 with a Reson 8160 multibeam sonar system (50 kHz). This data set was supplemented in 2004 with a Submetrix 2000 phase-measuring swath sonar (117kHz) covering areas shallower than 80 m water depth [*Tempera*, 2008; *Tempera et al.*, 2012] and additional multibeam lines collected over Faial's shelf edge using a Simrad EM710 in 2008 (EMEPC, data courtesy). The remaining gaps were filled with single-beam data collected in 2001 concurrently with the seismic reflection survey. A bathymetric mosaic compilation (in which grid nodes were assigned according to the highest quality data type where swaths overlap) was produced from these four data sets with a cell size of 10 m for the multibeam data and 50 m for the single-beam data. Figure 4 shows the surveys and Figure 5 the resulting bathymetry. Acoustic backscatter data recorded with the multibeam were processed with CARIS SIPS, including corrections of the geometry and the systematic intensity variations across swaths due to signal spreading, attenuation, beam pattern, etc. The final backscatter mosaics for this work were produced at a resolution of 10 m.

3.3. Sediment Sampling

[15] Superficial sediment sampling was conducted in November 2003, aboard the R/V *Arquipélago* [*Quartau et al.*, 2005]. Thirty-five stations were sampled using a box-corer (Figure 4). Grain size data were obtained using a dry sieving technique for material coarser than -1Φ (2 mm) and a Coulter Counter LS-230 for finer-grained material (<2 mm). The dry sieving was carried out over intervals of 1Φ ($-5\ \Phi$, $-4\ \Phi$, $-3\ \Phi$, $-2\ \Phi$ and $-1\ \Phi$ sieves). Both data sets were then merged to produce composite grain-size distributions.

3.4. Seafloor Imagery

[16] Visual ground-truthing of the seafloor with video imagery was accomplished using a VideoRay Explorer ROV in the summer of 2004 and a Tritech MD4000 drop-down camera in the summer of 2005 [*Tempera*, 2008]. The ROV operations were conducted down to ~60 m, while the vessel was at anchor. The drop-down camera was operated down to 180 m depth, along transects aimed at obtaining

cross-shore profiles while the vessel was left to drift. For most of the survey, videos were taken at 2 m from the substrate, which was sufficiently close to discriminate the seafloor type down to depths of ca. 100 m due to good sunlight penetration and high performance of the camera in low light conditions. In deeper areas, illumination relied on two camera LED lights, which provided sufficient light for ground distances less than 1 m. Since neither the ROV nor the drop-down camera were deployed with an underwater positioning system (e.g., USBL), their position was based on the vessel navigation. When cable drag and/or divergence from the boat track occurred, annotations of the length of cable deployed and a visual estimate of the cable-slanting angle to the vertical were used to do lay-back corrections.

3.4. GPS Positioning

[17] Differential GPS-accuracy positioning characterizes the 2003 and 2008 multibeam surveys and 27% of the phase-measuring swathe sonar survey conducted in 2004. The regular GPS precision characterizing the remaining data was still deemed sufficient for the scale at which features were analyzed. According to the *U.S. Department of Defense* [2001] regular GPS has featured a horizontal accuracy of ~8 m (95% RMS) subsequent to Selective Availability discontinuation.

4. Data Interpretation

4.1. Multibeam Bathymetry and Backscatter

[18] Processed backscatter mosaics were imported into a GIS and plotted with an inverted greyscale (black corresponding to high backscatter). Hillshade maps were derived from the bathymetry to highlight morphologic details. Seabed type interpretations have been made based on distinctive patterns expressed in the bathymetry, seabed gradient and tonal and textural properties of the backscatter. Smooth-surfaced sandy substrates appear light gray and homogeneous, as they are relatively weak acoustic scatterers here, possibly because the rocky outcrops are more strongly backscattering and dominate the image contrast. Rocky substrates are common in higher gradient areas and show the darkest patterns due to their high acoustic backscattering. Backscatter quality, and thus the ability to distinguish seabed types, significantly declined down the island slopes due to increasing water depth and artifacts generated by considerable across track changes in grazing angle associated with surveying parallel to a steep seafloor.

4.2. Classification of Chirp Echo Types

[19] Five different echo types (Table 1) were interpreted from the chirp profiles following the characteristics identified by *Damuth* [1980] and *Pratson and Laine* [1989]. They have been grouped into the following four classes.

4.2.1. Distinct Bottom Echoes

[20] Type I: Sharp, continuous, bottom echo with no or few diffuse sub-bottom reflectors (Figures 6a and 6b).

4.2.2. Indistinct Bottom Echoes

[21] Type II: Prolonged, continuous, echo with no apparent sub-bottom reflectors (Figures 6b and 6d).

4.2.3. Hyperbolic Bottom Echoes

[22] Type III-A: This type of echo shows regular, very intense overlapping hyperbolae with little varying vertex elevations and very prolonged echoes without sub-bottom reflectors. Each hyperbola is generally less than 3 m in relief and 1–2 m in wavelength (Figure 6a).

[23] Type III-B: This type of echo shows more irregular hyperbolae, which don't overlap and exhibit more greatly varying vertex elevations than echo type III-A. Each hyperbola is generally less than 10 m in relief and 50 m in wavelength (Figure 6b). It also shows a very prolonged echo without sub-bottom reflectors.

4.2.4. Composite Bottom Echoes

[24] Type IV: This type of echo does not easily fall into the general categories described above, being commonly a combination of more than one single type of echo, particularly a combination of echoes I, II, III-A and III-B (Figure 6c).

4.3. Sediment Texture

[25] Where the geophysical data suggested the presence of sandy sediments (echo type I and low backscatter), samples were taken and granulometric analysis performed. According to the Udden-Wentworth scale [*Wentworth*, 1922], 54% of the samples are medium sands, 17% are coarse sands, 26% are very coarse sands and 3% are granules. The sediments are angular to very angular [*Powers*,

Table 1. Character, Location and Interpretation of the Morphological Features of Faial's Shelf

Chirp Echo Class and Type	Multibeam	Video Imagery	Sediment Sampling	General Distribution	Process Interpretation
		I. Distinct			
Sharp continuous echo	Smooth-surfaced substrates; Light gray and homogeneous backscatter	Sands and gravels covering the seafloor	Sands and Gravels	Middle to outer shelf; more rarely nearshore	Depositional
		II. Indistinct			
Prolonged and continuous echo	Relatively smooth-surfaced substrates; Light gray and less-homogeneous backscatter	Pebbles and cobbles covering the seafloor		Shelf sectors A1 and A2	Depositional
		III. Hyperbolic			
III-A: Small and regular overlapping hyperbola	High gradient surface substrates; Dark gray backscatter	Rounded boulder-size sediments covering the seafloor		Nearshore to middle shelf	Erosive; Mass-wasting
III-B: Medium and irregular overlapping hyperbola	High gradient and very irregular surface substrates; Dark gray backscatter Lava flow morphology	Lava flows		Nearshore to middle shelf	Volcanic progradation
		IV. Composite			
Intercalation of distinct, indistinct and hyperbolic echoes	Alternation between smooth and irregular surfaced substrates and light and dark gray backscatter	Lava flows interspersed with sand to boulder-size sediments		Shelf sectors A1 and A2	Volcanic progradation; Erosive; Depositional

1953], moderately sorted to poorly sorted and symmetrical to coarse skewed. The calcium carbonate composition of the superficial sediments was also determined using a digestion method [*Müller and Gastner*, 1971]. Sediment samples are mainly composed of volcaniclastic sand, with lesser carbonate skeletal particles (1–22%).

4.4. Echo-Types Interpretation and Distribution

[26] The line-based interpretations of echo types were compiled, also supported by the remaining data (Figures 6a to 6j), to form an echo character map (Figure 7). Echo-type I is generally located between 30 and 50 m depths and the shelf edge and is commonly bounded upslope by echo type III-A. This echo type shows nearly flat or gently sloping topography near echo III-A, passing seaward to a convex downward break in slope to the shelf edge, which in some cases can reach gradients of more than 10° (Figure 6a). More rarely this echo type occurs near the shore, where it then tends to cover the entire shelf. According to *Damuth and Hayes* [1977], where the shelf is dominated by coarse-grained sediments, no sub-bottom reflectors appear in the echograms (which is the case for most of the type I echoes), associated with strong attenuation. *Damuth* [1975] showed that more prolonged echoes with no sub-bottom reflectors (e.g., type II) are

Figure 6. Examples of chirp seismic lines (Figures 6a–6d) used to classify the five echo-character types identified. Letters in the upper part of the profiles refer to their orientation. (a) Types I and III-A. (b) Types I, II and III-B. (c) Type IV (the arrows show echoes of the type I to II while the remaining corresponds to the type III-A). (d) Type II. ROV and multibeam backscatter images (Figures 6e–6j) used to support the echo interpretation. (e) ROV image showing rounded boulders in an area classified as echo III-A from the chirp profile Figure 6a. (f) ROV image showing a sandy seafloor in an area classified as echo I from the chirp profile Figure 6a. (g) Backscatter image showing the area crossed by chirp profile Figure 6a and the transition from south to north of high (echo type III-A) to low backscatter (echo type I). (h) ROV image showing a lava surface in an area classified as echo III-B. (i) ROV image showing the typical surface of the area classified as echo IV from chirp profile Figure 6c. (j) Backscatter image showing the area crossed by chirp profile Figure 6b and the transition from high (echo type III-B) to low backscatter (echo type I and II). See Figure 7 for location of the seismic lines, ROV images and multibeam backscatter mosaics.

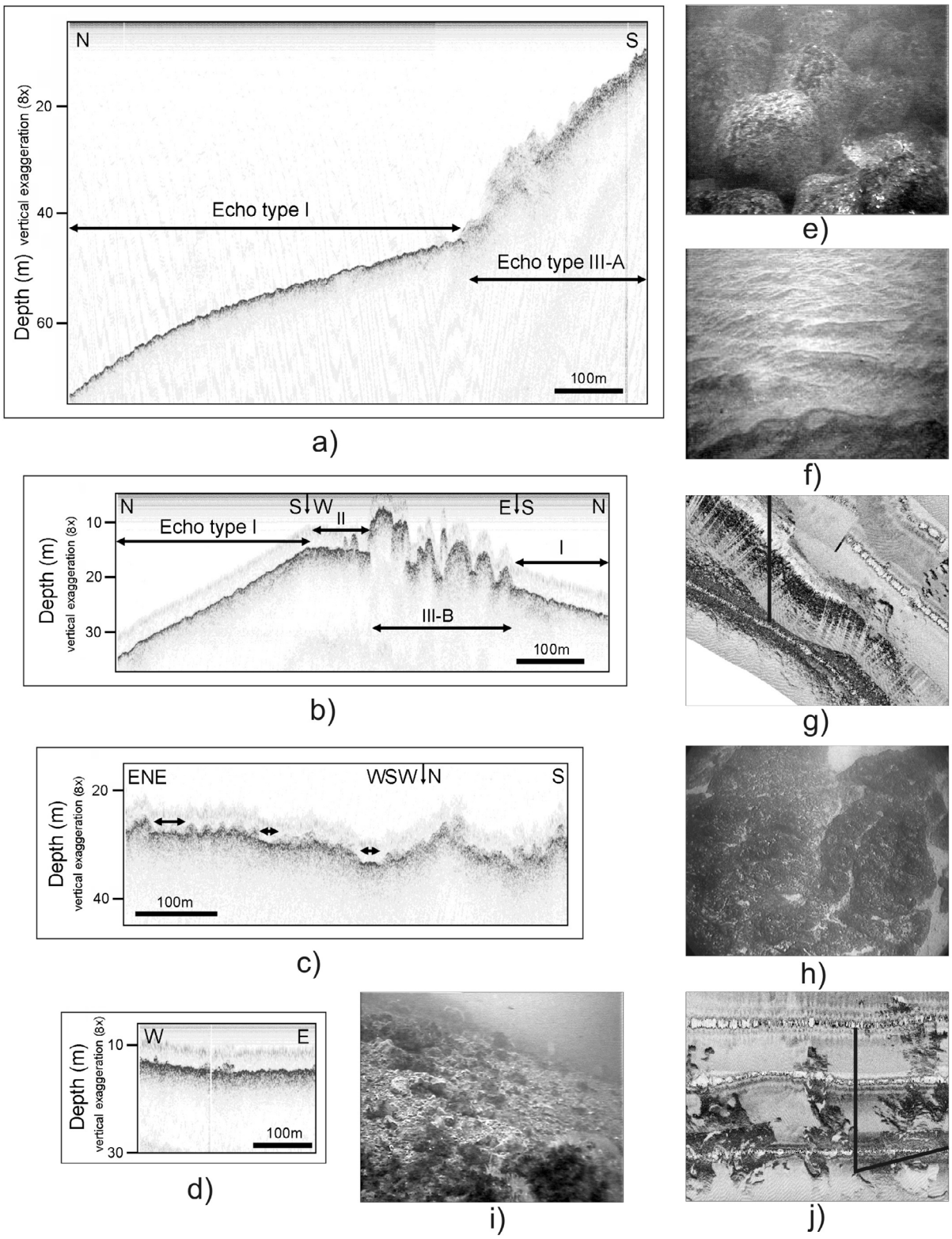
N
S
Depth (m) vertical exaggeration (8x)
20
40
60
Echo type I
Echo type III-A
100m
a)
e)
f)
N
S
W
II
E
S
N
Echo type I
I
III-B
100m
b)
g)
ENE
WSW
N
S
100m
c)
h)
W
E
100m
d)
i)
j)

Figure 6

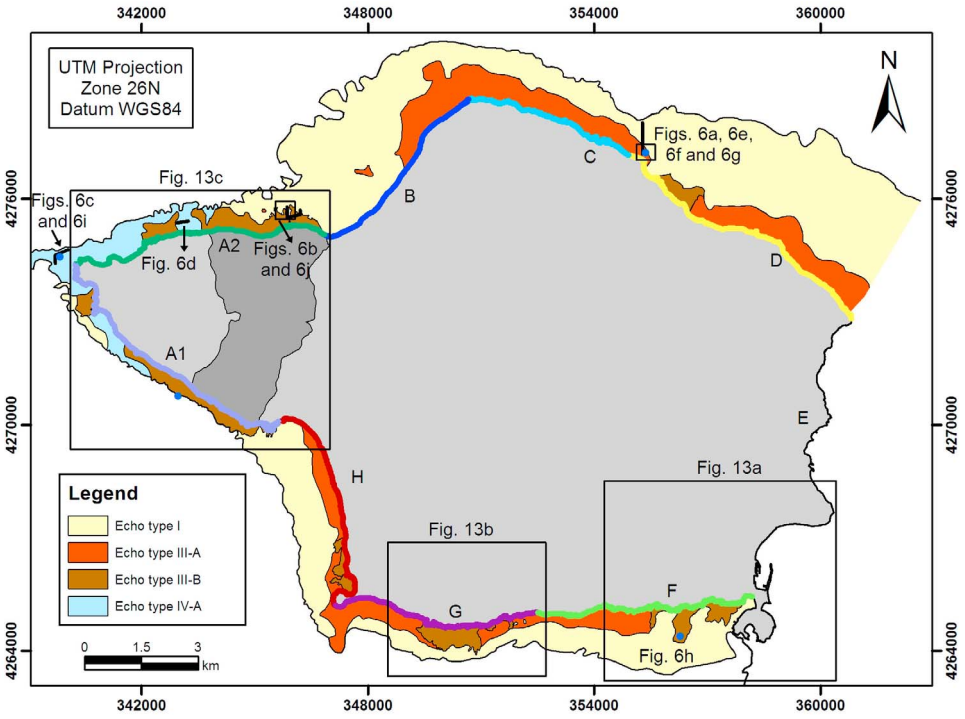

Figure 7. Map of chirp echo types. The different color lines bordering the coastline and accompanying letters represent different shelf sectors referred to in the text. The darker gray area onshore represents the historical lava flow of 1672 AC that extends offshore, mapped as echo type III-B. Black line depicts the shelf edge, black bold lines the chirp seismic profiles in Figure 6, blue dots the ROV images in Figure 6, small boxes the backscatter images in Figure 6 and big boxes the areas in Figure 13.

covered by even coarser sediments creating the prolonged echo from acoustic scattering. We thus expect to find sand and gravels associated with echo type I and pebbles and cobbles with echo type II, which was confirmed by the ROV images, multibeam backscatter and sampling (see Figures 6f, 6g, 6i and 6j).

[27] Echo-type III-A generally occurs from the coastline to 30–50 m depths, associated with steeper slopes and sometimes a stepped seabed morphology. Echo-type III-B generally appears nearshore, associated with echo type III-A (Figure 7). Hyperbolic echoes are either caused by rugged seafloor topography or by undulating seafloor surfaces [*Damuth*, 1980]. The strongly reflective single or irregular overlapping hyperbolae with widely varying vertex elevations above the seafloor are suggestive of basement highs or outcrops and have no relationship to sedimentary processes [*Damuth*, 1975, 1980]. Therefore, the small size and intense overlapping hyperbolae of echo type III-A represent returns from coarse clastic deposits comprising boulder-size blocks, as confirmed in video imagery (Figure 6e). Echo types III-B are caused by the presence of lava flows, confirmed by video imagery (Figure 6h). *Mitchell et al.* [2008] have shown a remarkable variety of submarine lava flows in Pico shelf that are very similar to the examples found here (Figure 6j).

4.5. Seismic Stratigraphy

[28] The boomer seismic profiles were interpreted using classic seismic stratigraphic methods [*Mitchum et al.*, 1977a, 1977b]. Only one seismic unit has been identified (Figure 8), limited at its base by a well-defined, continuous and high-amplitude reflection and at the top by the seafloor. The unit contains parallel reflections with low amplitude and medium lateral continuity. However, in some profiles it is possible to distinguish some reflections that are discordant with the internal reflections of the identified unit. Their lack of lateral continuity and low amplitude may be attributed to the poor resolution of the seismic data, or small density variations (acoustic impedance). Therefore, the application of traditional seismic stratigraphy techniques was limited and only one seismic unit was used to obtain the sedimentary deposits thickness

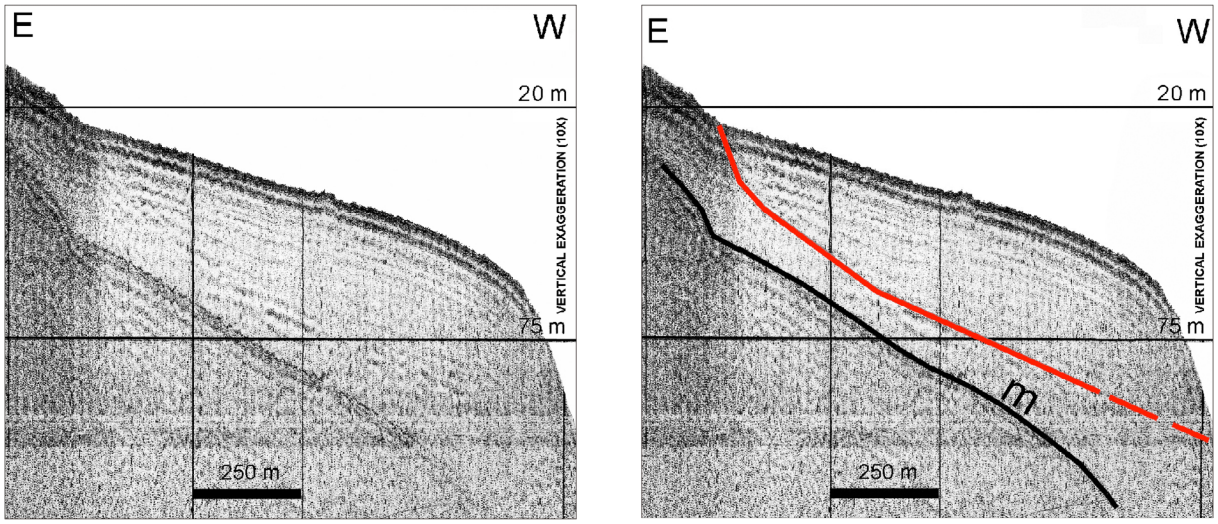

Figure 8. (left) Boomer seismic section and (right) its interpreted base of the sand body (red line) for the profile located in Figure 9 (P33). Annotation 'm' represents the multiple of the seafloor.

(Figure 9). Pale green areas in this figure represent regions where the signal was too poor to allow estimates of sedimentary thickness to be made. Sediment thicknesses were calculated from seismic two-way time using a sound velocity of 1800 m/s for coarse sands [*Hamilton and Bachman*, 1982].

4.6. Geological Interpretation and Morphological Mapping

[29] The interpretations of the individual geophysical and geological data sets were combined in a GIS to produce maps of the seafloor nature that permitted the discrimination of eight shelf sectors (A to H in Figures 7 and 9) based on the geological differences found onshore and offshore.

[30] Rocky substrate covers the majority of the nearshore areas up to 30–50 m depth, with median gradients ranging 3°–4°. Below these depths smooth sedimentary seabeds dominate and median gradients decrease to 2°. Between 70 and 120 m, median gradients increase sharply from 2° to 11° marking the transition from the shelf to the slope. The shelf edge is often a depositional feature and shows evidence of mass-wasting features. The following section looks at the nature and distribution of these morphologies.

4.6.1. Erosional Morphologies

4.6.1.1. Erosional Shelf

[31] The inner to middle shelf has extensive bedrock outcrops (Figure 7) forming a 0.2 to 0.8 km-wide belt extending from the coastline to 30–50 m depth (average 40 m). This rocky seafloor is often covered by very coarse volcaniclastic rounded sediments (mostly boulder size, Figure 6e) interspersed with a thin veneer of sandy sediment (below the resolution of the boomer system but interpretable from the swath sonar backscatter). In sectors B and H this belt is less developed and sometimes absent. These very coarse volcaniclastic deposits (Figure 6i) cover around half of sectors A1 and A2. In sectors B, C, D, F, G and H, often, below 40m, the shelf consists of a smooth erosion platform covered by sandy sedimentary bodies (see section 4.6.2.1).

4.6.1.2. Mass-Wasting Features

[32] Embayments indicating mass-wasting are noticeable at or near the shelf break in sectors B, G and H (Figures 10a and 10b), with slopes within the embayment generally smoother than those in adjacent slope areas, which approach the 30° gradients of angular talus ramps [*Mitchell et al.*, 2000]. In contrast, the shelf edges of A1 and A2 seldom show embayments and are deeply indented by gullies (Figures 10a and 10c).

4.6.2. Depositional Morphologies

4.6.2.1. Sandy Sedimentary Bodies

[33] The thickness of the sandy sedimentary bodies interpreted from the boomer seismic data is poorly

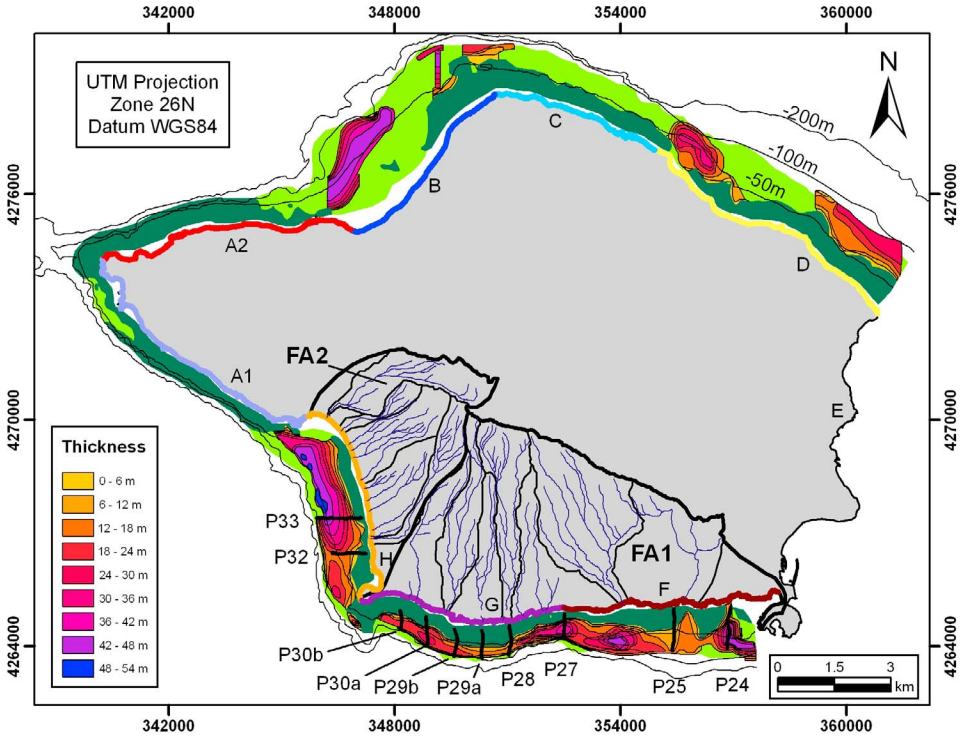

Figure 9. Seabed type and sediment thickness map based on the boomer seismic data. The dark-green areas correspond to rocky outcrops. Yellow to blue colors represent sediment thickness. Sediment thickness data are unavailable in the light green areas. The light black lines correspond to bathymetric contours. The different color toned lines bordering the coastline and the accompanying letters represent the different shelf sectors referred to in the text. Black bold lines and respective labels locate the boomer seismic profiles in Figures 8 and 11. Black bold lines onshore represent the two areas (FA1 and FA2) draining respectively to shelf sectors F and G and H. Lighter black lines represent the delimitation of the individual hydrographic basins and blue lines delineate the streams.

mapped in sectors B, C and D but well constrained in F, G and H (Figure 9). In sectors A1 and A2, these bodies are only present in a small area south of the Capelinhos volcano while in the remaining areas the sand forms a thin veneer on the rocky substrate without an organized structure.

[34] These bodies typically trend parallel to the shore and exhibit a cross-shore sigmoidal shape in profile (Figures 8 and 9). They are thicker (30 m average) in the middle to outer shelf (50–60 m depth). Where internal reflections are present, they have a typical aggradational geometry and thin out toward the shore and offshore terminations. In C, D, F and G the bodies end toward rocky outcrops at ~40 m depth with onlap terminations. In the offshore direction, the unit almost disappears at the shelf edge. Although the offshore terminations are not well imaged in the seismic profiles, they appear to downlap, mainly inferred by the thinning of the unit. Even if all the sectors were not well mapped, the bodies appear better developed in sectors B and H where they can reach 40–50 m in thickness. There they also onlap against rocky outcrops at shallower depths than typical, sometimes even reaching the coastline.

4.6.3. Volcanic Morphologies

4.6.3.1. Lava Flows

[35] Irregular rocky features with dendritic termini have been interpreted as lava flows in nearshore areas of sectors A1, A2, D, F, G and H (Figures 6j, 7 and in front of arrows in Figure 10a). These are comparable to the Pico lava flows [*Mitchell et al.*, 2008] with no obvious signs of post-emplacement erosion. The majority only reach the inner shelf, but two extend as far as the middle shelf (sectors F and G). The historical lava flows of the Capelo Peninsula (1672 AC) have flowed onto the shelf in both sectors A1 and A2. The southerly flow crosses the narrow shelf reaching the shelf edge (Figures 7 and 10a) whereas the northerly flow only reaches

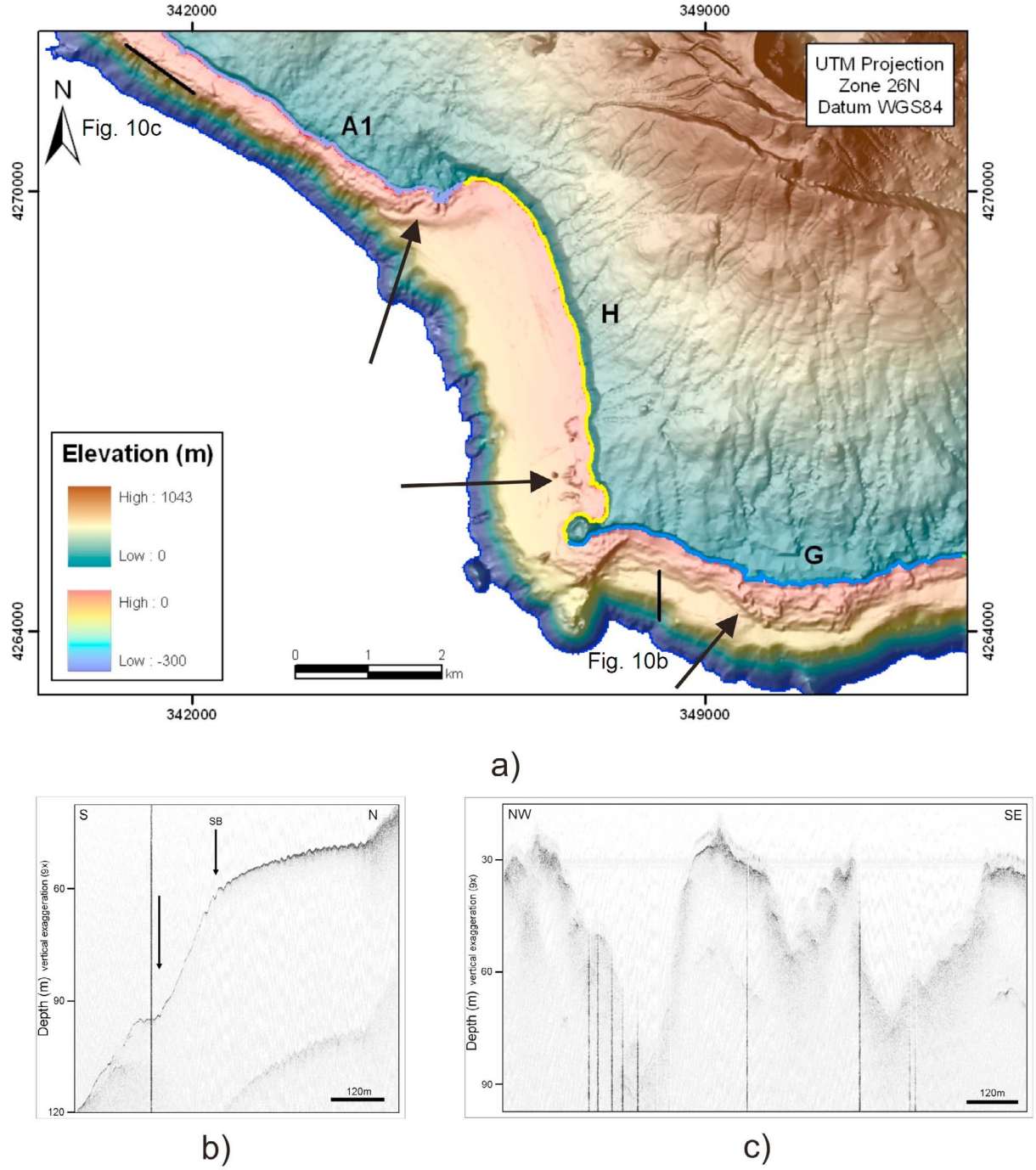

Figure 10. Examples of mass-wasting features near the shelf edge and lava progradation (marked by arrows). (a) Bathymetric map showing the shelf edge in sectors F and G highly embayed, and in sector A1 less strongly embayed by gullying. (b) Chirp seismic profile (location in Figure 10a) showing a cross-shore section over one large embayment interpreted as a slump: Immediately below the shelfbreak (SB) there is a scarp, bounded downslope by an irregular blocky mass. (c) Chirp seismic profile (location in Figure10a) showing an along-shore section of the shelf edge indented by gullies.

41 m, very near the shelf break in the NW branch of the flow (Figure 7).

5. Discussion

5.1. Erosion Platform

[36] Following the phase of active volcanism, shelves widen progressively, so that shelf widths increase with edifice age as observed elsewhere [*Ablay and Hurlimann*, 2000; *Le Friant et al.*, 2004; *Llanes et al.*, 2009; *Menard*, 1983, 1986; *Mitchell et al.*, 2003a]. *Quartau et al.* [2010] recognized a similar trend in Faial and attempted to quantify the role of wave abrasion on the development of its shelf. A wave erosion model and a eustatic record of glacially induced oscillations of sea level were used to reproduce the morphologies of different sectors of Faial's shelf. Results showed that most parts of the shelf of Faial are the product of wave erosion. Shelf width is related to the amount of time that coastal sectors have been exposed to waves [*Quartau et al.*, 2010, Figure 13] but also to the frequency and significant height of waves (interpreted from differences in width between sectors of similar age, e.g., sectors B, C, G, H on the Caldeira stratovolcano and A1 and A2 on the Capelo Peninsula) [*Quartau et al.*, 2010, Figure 14]. They also showed that discrepancies between modeled and the actual shelf profiles are mostly due to recent volcanic progradation onto the shelf, sediment infilling and tectonic vertical movements. Nevertheless, the dominance of wave erosion over other processes makes shelf morphology very useful to asses the evolution of young islands which is often based only on their subaerial parts.

[37] The nearshore shelf areas consist of rocky seafloor, mostly covered by coarse clastic deposits. Morphologically these deposits show nearshore terraces that are moderately dipping (typically 3°–7°), with a rugged small-scale and sometimes stepping morphology (Figure 11). Seaward of the terraces, the seabed dips 5°–14° with its offshore limits buried by the sandy sedimentary bodies at around 40 m water depth. These sediments cover the smooth rocky basement which resulted from wave erosion [*Quartau*, 2007; *Quartau et al.*, 2010]. The platform dips gradually beneath the sediments to the erosional shelf edge where its gradient declines to 1°–4°, before steepening on the island slope. The presence of rounded coarse clastic deposits in the nearshore areas can be explained by erosion of lava flows that have prograded onto the shelf. These lava flows were probably emplaced before the Holocene and eroded during sea level fluctuations, otherwise their fine lava structures would have been preserved [*Mitchell et al.*, 2008]. Furthermore, the surface in these nearshore areas is rather irregular when compared with the wave erosional basement under the sandy sedimentary bodies, perhaps because it has been modified by wave erosion only throughout the last post-glacial sea level rise. The steeper gradient of the seafloor (3°–7°) when compared with the erosional platform under the sandy sediments (1°–4°) is also further evidence of its youth [*Mitchell et al.*, 2012]. A good example of this is the NE part of sector B that shows coarse clastic deposits up to −40 m. The coastline changes from concave in the SW, with cliff heights of 300 m to convex in the NE, with cliff heights around 100 m. Likewise, shelf width decreases from 3 km to 2 km SW to NE (Figure 12). Lava progradation is the likely explanation for this morphological change from SW to NE and some of the possible sources can be found onshore with well preserved cones (V1 and V2 in Figure 12). These two are probably not enough to justify all the coastal progradation here but other cones might have contributed that are now buried by the pyroclasts of Caldeira Formation or eroded by the last sea level rise. One of them (V2) has been K/Ar dated by *Féraud* [1980] with 21 ± 10 ka which suggests that its activity together with others might have been responsible for extending the previous coastline offshore during the last sea level lowstand. Later, during the most recent sea level rise their products were eroded to form the coarse clastic deposits. Therefore, the nearshore rugged terraces are interpreted as the eroded topset units of a lava delta whereas the seaward higher gradient area is interpreted as the eroded foreset units. A typical example is shown in profile P27 (Figure 11). The other profiles are intermediate cases between that and the other end-member (P25), which suggests almost continuity above and below the sandy clinoforms. In this case (P25), the erosion platform above and below the sediments was probably formed at the same time. Some of these deposits could also be formed by cliff retreat. However, given that these are generally extensive and backed by high cliffs, coastline erosion would produce a lot of coarse material, which in turn would have protected the cliffs from wave erosion. Therefore, it is unlikely, given that platform width is often inversely correlated with cliff height [*Dickson*, 2004], that these deposits were produced during the last sea level rise by a retreat of 0.2–0.8 km of the

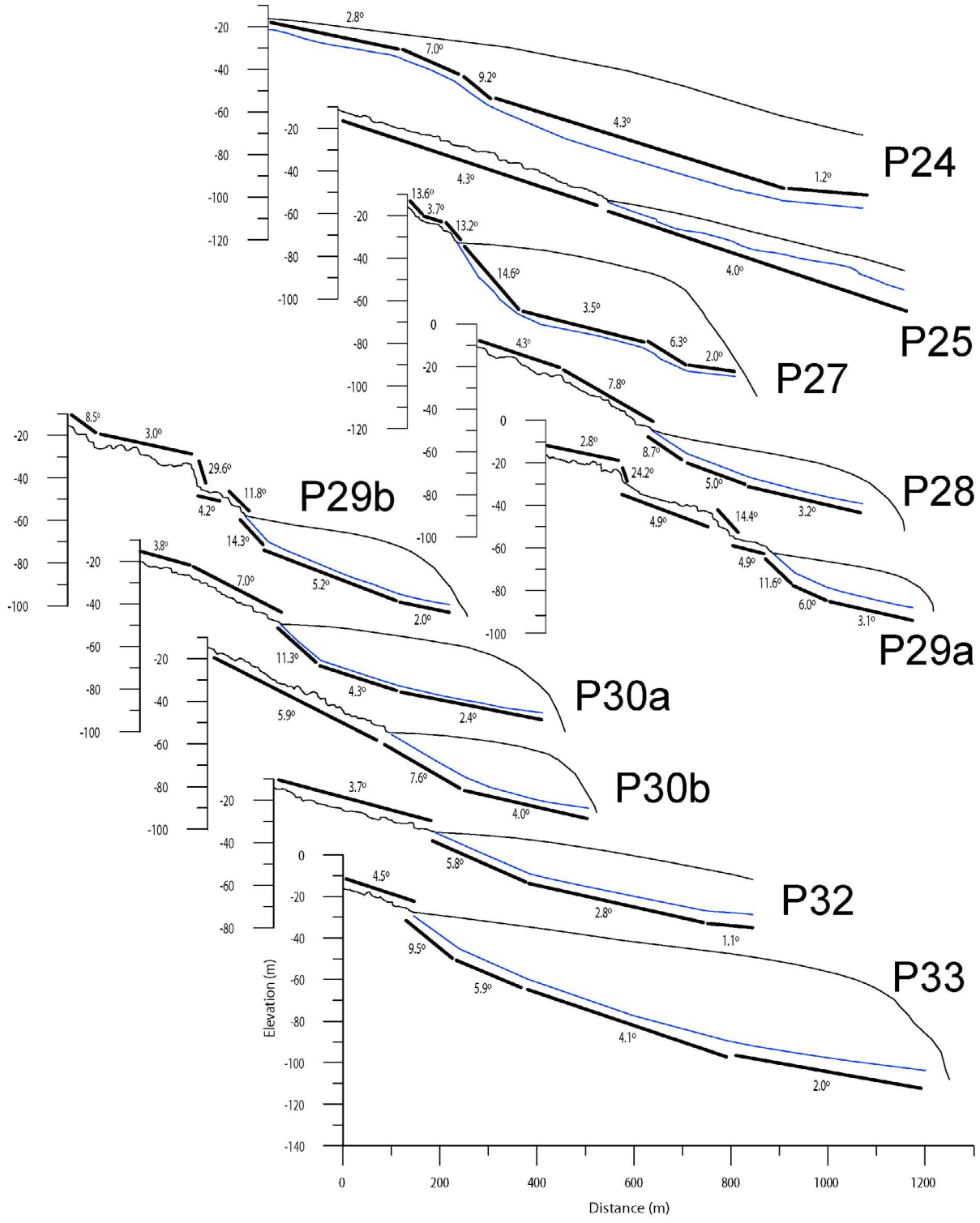

Figure 11. Depth-converted interpretations of the shore-normal sections of the boomer profiles showing the seabed (black line) and acoustic basement reflections (blue line). Bold black lines and respective values represent the segments of the seabed and acoustic basement reflections selected for measuring their gradient in degrees. Labels in front of the sections are used to locate seismic profiles in Figure 9.

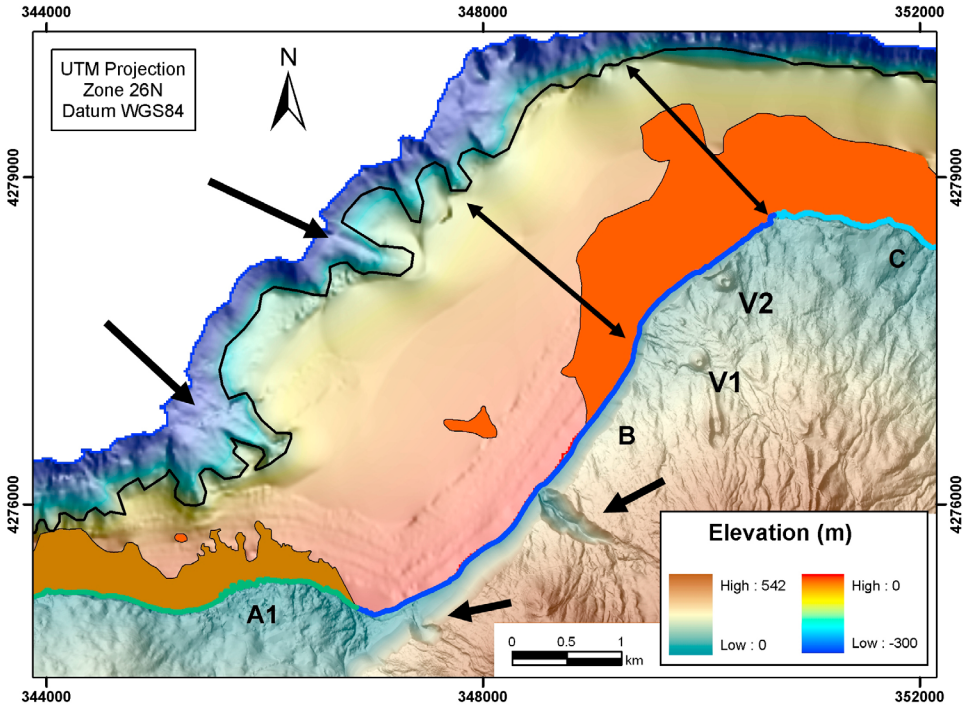

Figure 12. Location of some recent volcanic cones (V1 and V2) that were probably responsible for the progradation of the island onto the shelf in the NE part of sector B. Two arrows delimit the area where the sector B edifice is interpreted to have prograded to the NW. Other arrows mark valleys due to streams at the coastline and canyons at the shelf edge, both striking WNW-ESE. Areas and lines with single color offshore have the same legend as Figure 7.

coastline. Some profiles show a nearshore step-like morphology (P27, P29a and P29b) suggesting that they may have been formed by the piling up of several lava flows. Their exposed surface has subsequently been eroded and covered by rock debris but maintained a stacked morphology. Another possible explanation for the presence of these nearshore terraces could be sea level stillstands. Indeed, the wave erosion model produced nearshore terraces (up to −20 m) for sectors B to H [*Quartau et al.*, 2010, Figures 11 and 12]. However, the surface irregularity as well as the difference between the model (wider) and the actual shelf width suggests that these areas are the result of lava flow progradation and subsequent erosion.

5.2. Lava Flows

[38] Although in older islands erosion may dominate, the shelf morphology in young islands reflects a competition between processes enlarging the shelf and those infilling it. Renewed volcanism may partially or completely fill the space left by wave incision. Evidence of recent seaward volcanic progradation have been found on sectors A1, A2, D, F, G and H. The well-preserved lava flows (mapped in Figure 7 and examples in Figure 10a) suggest that these structures were probably emplaced after the Holocene transgression had submerged the shelf. It is unlikely that these structures are pre-Holocene subaerial flows emplaced during lower sea levels and have survived surf erosion during sea level rise in such an energetic environment; here, for instance, wave erosion during last sea level rise has formed a 400–700 m wide shelf on sectors A1 and A2 [*Quartau et al.*, 2010]. In some of these submarine lava flows we were able to identify their possible onshore sources (Figures 13a, 13b and 13c), which supports the hypothesis that these structures result from flows crossing coastal cliffs. In others we were unable to identify the sources and nearshore tube openings or vents are more likely explanations for their origin. Compared with Pico Island's shelf there are relatively few lava flows, which is a consequence of Faial's more mature shelf where wave erosion dominates.

5.3. Sandy Sedimentary Deposits

[39] Sedimentary bodies have been found in all shelf sectors. They show clinoform geometries without

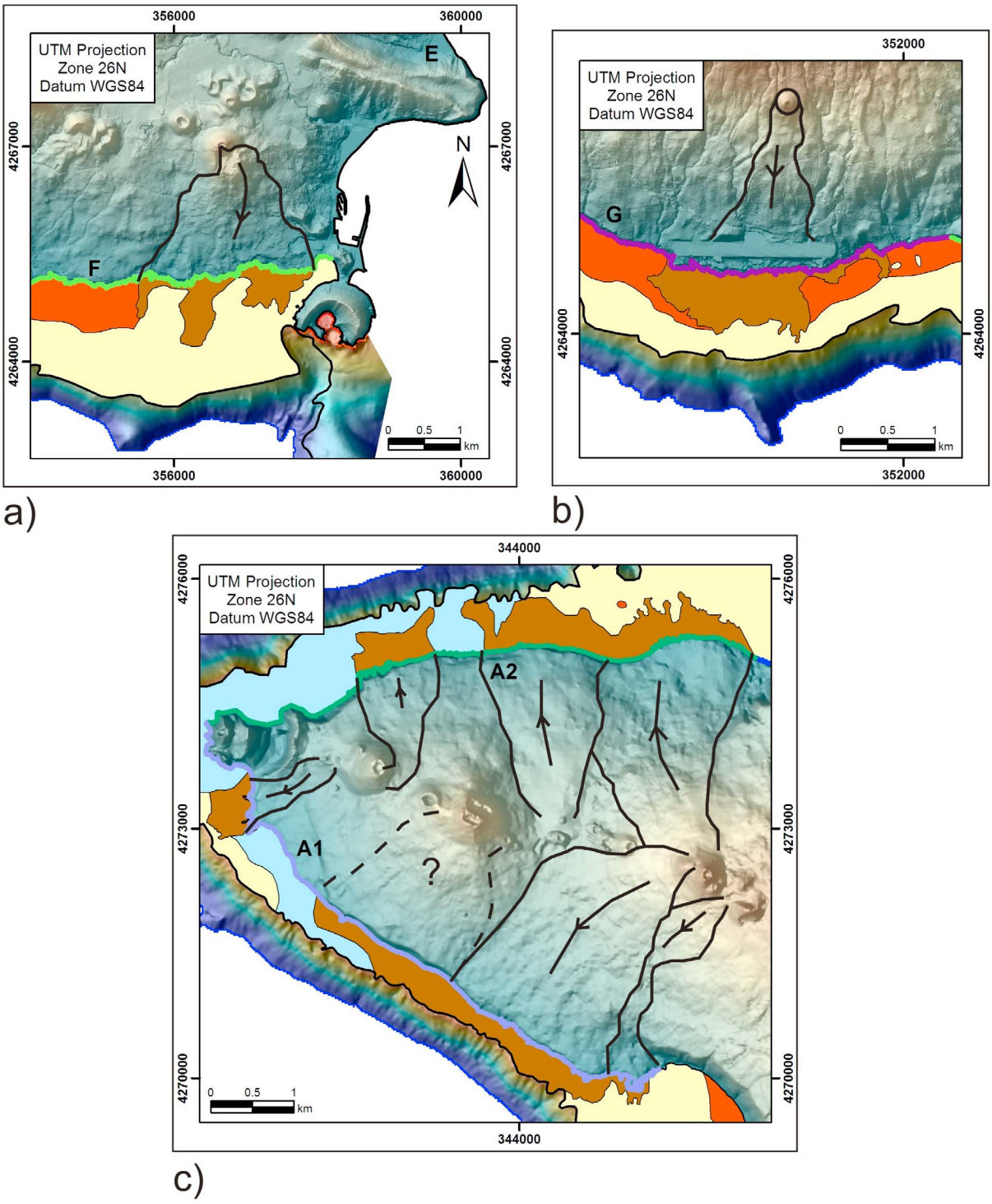

Figure 13. Onshore sources of the submarine lava flows based on the work of *Madeira* [1998] and interpretation of the Faial Island DEM. Areas and lines with single color offshore have the same legend as Figure 7. Location of Figures 13a, 13b and 13c can be found in Figure 7.

bottomset, with aggradation in the middle shelf and apparent progradational geometry near the shelf edge. Aggradational geometry normally occurs when sediment supply equals accommodation, and progradation when sediment supply exceeds accommodation. In very energetic environments, such as the Azores, these bodies are interpreted to be formed by storm-induced downwelling currents

that transport coastal sediments offshore as observed in other energetic environments [*Chiocci and Romagnoli*, 2004; *Field and Roy*, 1984; *Hernández-Molina et al.*, 2000; *Nittrouer and Wright*, 1994]. These offshore directed currents were measured by *Youssef* [2005] in Faial over one year, who found that 80% of the higher current speeds (reaching 2 m/s) were associated with high-energy waves and directed normal to the shore. Therefore, it appears that these currents move sediment from the coastline to the middle and outer shelf leaving nearshore areas depleted. In the middle shelf they aggrade, because there is still space for accommodating sediments, while near the shelf edge they prograde. Although these deposits have not been cored and dated, the lack of major internal reflectors suggest that subaerial exposure, erosional events and subsequent burying by younger deposits associated with sea level changes have not occurred. Thus, these deposits probably started forming around 6.5 ka, when sea level rose to its maximum level in Iberia, the nearest sea level record to the Azores [*Dabrio et al.*, 2000; *Hernández-Molina et al.*, 1994]. This interpretation is similar to those of other volcanic island shelf deposits [*Chiocci and Romagnoli*, 2004; *Grossman et al.*, 2006].

5.3.1. Sources of Shelf Sediment Supply

[40] The submarine deposits in sectors F, G and H were almost completely mapped (Figure 9) and for that reason their volume can be measured and compared with the amount of sediment produced onshore during the last 6.5 ka. There are basically three types of possible onshore sources identified in the Faial Island:

[41] 1. Eruptive activity, associated with explosive volcanism and lava progradation into the sea. Although a significant number of recent lava flows were identified as having entered the sea (Figure 7), the quantity of hyaloclastite produced due to lava quenching is difficult to assess. On the other hand, the amount of pyroclastic explosive material released to the sea in the last 16 ka is relatively easy to calculate based on the measured thickness of the onshore deposits from the work of *Pacheco* [2001] and extrapolating them to the offshore. He identified two pyroclastic deposits younger than 6.5 ka that projected material south of the island, respectively C4 and C5-C6 that we extrapolated offshore, obtaining an output of 43×10^6 of m^3 (37×10^6 of m^3 to shelf sector F and G and 6×10^6 of m^3 to sector H).

[42] 2. Cliff erosion, mainly related to wave forcing. Rates of modern coastal erosion can be high around volcanic islands depending on the timescale of measurement and the materials [*Quartau et al.*, 2010]. Since there are no short-term rates known for Faial we used the lowest, average and highest measured retreat rates (0.01, 0.21 and 1.07 m/year respectively) from an analysis of 44 years of aerial photos of the coasts of São Miguel [*Borges*, 2003], an island in the Azores that is similar to Faial in terms of volcanic deposits and wave energy. Calculations over 6.5 ka represent 24/510/2604 (min/avg/max) $\times 10^6$ of m^3 of sediments for sectors F and G and 70/1460/7436 (min/avg/max) $\times 10^6$ of m^3 of sediments for sector H. We used a typical sand dry bulk density of 2.5 g/cm^3 and a typical density of basalt of 3.0 g/cm^3 in these calculations.

[43] 3. Subaerial erosion in drainage basins. Similarly, there are no records of the subaerial erosion in the hydrographic basins of Faial Island. However, it is possible to infer erosion rates from the work of *Louvat and Allègre* [1998] on S. Miguel Island. They estimated erosion rates of riverine mechanical erosion ($\pm$300–500 ton/ km^2/year) in three hydrographic basins, whose hydrologic parameters (surface area, stream length, maximum elevation and runoff) are somewhat greater than those from Faial (Figure 9 and Table 2). If streams carry more sediment as they mature and as drainage density increases, on the other hand, loose volcanic materials such as pyroclastic deposits covering the basins of Faial will be more susceptible to erosion. However, these deposits are typically very thin, (a few meters thick) and the streams are only a few meters below them. To evaluate this sediment contribution, the lowest and the highest erosion rate values of S. Miguel were used for the calculations (a compromise between rapid erosion of friable materials and slower erosion of deeper rocks). We obtained respectively minimum and maximum values for sectors F and G (15 and 43×10^6 of m^3) and H (7 and 20×10^6 of m^3).

[44] We have also considered the submarine biological productivity in the calculations. Average percentage of calcium carbonate (bioclasts) measured from samples of sector H was 2% and from sectors F and G around 14%. Table 3 is a resume of the calculations made and the obvious conclusion is that most of the volcaniclastic material on the shelf results from wave erosion with decreasing contributions from subaerial erosion and explosive volcanism. It is also evident that we should expect average to high wave erosion rates on these sectors (Table 3), since these are subject to medium to high wave energies (Figure 3). Therefore, many of the sediments have probably crossed the shelf onto the

Table 2. Calculation of Subaerial Erosion Rates in Faial Hydrographic Basins (FA1 and FA2) Based on Rates From *Louvat and Allègre* [1998] of S. Miguel (SM4, SM9 and SM10)

	Known From the Literature				
	SM4	SM9	SM10	FA1[c]	FA2[c]
Area (km^2)[a]	20	10	17	4.5	2.2
Drainage Density[a]	5.3	5.5	4.7	1.8	3.7
Average/Maximum Elevation (m)[a]	422/884	483/872	415/910	243/888	487/1040
Runoff (mm/year)[a]	1063	1220	617	81	925
Total Yield (ton/km^2/year)[b]	525 ± 72	184 ± 45	325 ± 72	x	x
	Estimation				
	FA1			FA2	
Area (km^2)	15			33	
Erosion Rate (min/max in ton/km^2/year)	170/500			170/500	
Time Span (years)	6500			6500	
Total Yield (min/max in $\times 10^6$ m^3)	7/20			15/43	

[a]Data from *DROTRH- IA* [2001].
[b]Data from *Louvat and Allègre* [1998].
[c]Values from individual subbasins inside the areas FA1 and FA2.

slope, because the volumes presently on the shelf are significantly lower than those produced by average to high wave erosion rates.

[45] *Menard* [1983, 1986] showed striking examples of asymmetric erosion of high and large islands due to the effect of rainfall and waves, which work together to reinforce the windward erosion of islands. However, in Faial precipitation is primarily related to altitude and in small and intermediate-size islands such as here, waves are more effective erosional agents than streams. This is confirmed by the calculations and previous work [*Quartau et al.*, 2010]. Therefore, differences in thickness and area of the clinoform deposits are probably more related to the wave energy exposure. Indeed, the sectors more exposed to wave erosion (B and H) have higher cliffs and wider shelves (Table 4). Therefore, these coastlines can produce more sediment, which in turn can occupy a larger area of the shelf. Thus, the transition from the rocky seafloor to the sandy clinoforms occurs at shallower depths (Table 4). Shelf sector D is an exception because it is the widest, although it is relatively more protected from wave energy than the west-facing sectors. Unfortunately, it is impossible to compare the thickness of its deposits because of the missing seismic data. However, its greater width is related to its age which is almost the double of the age of sectors B and H. Sector F is also wider when compared to sector C and G, although exposed to a similar wave regime, but this part of the shelf appears to be as old as sector D and has been modified by lava progradation that most likely has produced hyaloclastites [*Quartau et al.*, 2010], which accounts for the volumetric shelf deposits here. On the other side, sectors A1 and A2 are the narrowest (400–700 m on average) and lack significant sedimentary deposits. This probably arises because stages of volcanic repose (when erosion and sedimentation are possible) have alternated with episodes of seaward volcanic progradation during the last 16 ka, potentially burying older deposits. In addition, these sectors are the narrowest and the more exposed to wave energy, thus

Table 3. Comparison of the Offshore Measured Volumes With the Calculated Onshore Sources of Sediments

	Submarine Volumes (X 10^6 m^3)			Subaerial Sources (X 10^6 m^3)		
	Total Volume of Sediments	Volume of Bioclasts on Sediments	Volume of Volcaniclast Sediments	Explosive Volcanism	Wave Erosion (min/avg/max)	Hydrographic Basins (min/max)
Sectors F and G	106	15	91	37	23/510/2604	15/43
Sectors H	103	2	101	6	70/1460/7436	7/20

Table 4 (Sample). Shelf Width, Cliff Height and Depth of the Base of Sandy Clinoforms of the Sectors Defined for the Faial Island in Meters[a] [The full Table [NN] is available in the HTML version of this article]

	Sector A1					Sector A2					Sector B				
	Min	P25	P50	P75	Max	Min	P25	P50	P75	Max	Min	P25	P50	P75	Max
Shelf Width	172	342	421	491	727	440	553	675	967	1174	1739	2100	2329	2787	3042
Cliff Height	0	8	19	39	73	7	22	33	63	121	62	103	224	281	321
Depth of the Base of Clinoforms	11	16	20	24	26						0	1	33	48	68

	Sector C					Sector D					Sector F	
	Min	P25	P50	P75	Max	Min	P25	P50	P75	Max	Min	P25
Shelf Width	1034	1155	1238	1370	1434	1401	2716	2984	3128	3290	1073	1365
Cliff Height	28	34	43	51	60	23	80	113	137	161	0	0
Depth of the Base of Clinoforms	42	46	50	57	62	2	6	49	58	64	6	16

	Sector F			Sector G					Sector H				
	P50	P75	Max	Min	P25	P50	P75	Max	Min	P25	P50	P75	Max
Shelf Width	1615	1712	1827	773	874	914	976	1069	1239	1314	1379	1424	1728
Cliff Height	6	11	35	0	0	11	26	56	69	132	186	231	259
Depth of the Base of Clinoforms	27	39	52	26	40	45	50	58	0	15	23	29	44

[a]P25, P50, P75 represent the 25th 50th and 75th percentiles.

downwelling offshore currents are probably more effective in sweeping the sediments to the slope.

5.4. Preservation Potential of Depositional Sequences in Volcanic Insular Shelves

[46] The sedimentary bodies in the shelf are interpreted as highstand deposits although most of the island shelf is quite old. Shelf sectors D and F are undoubtedly older than 470 ka [*Quartau et al.*, 2010] because the end of Ribeirinha volcanism was about 580 ka [*Madeira*, 1998]. Sectors B, C, G and H must have been carved after the main active phase of Cedros Volcanic Complex, which probably occurred between 470 and 100–70 ka [*Madeira*, 1998]. According to sequence stratigraphic models one should expect three to five system tracts within a depositional system [*Catuneanu*, 2002] associated to changes in the direction of shoreline shift from regression to transgression and vice versa. Since other systems tracts associated with sea level changes normally described for continental shelves (e.g., lowstand and transgressive systems tracts) are not present here, conditions on this volcanic island shelf appear not to have favored preservation of older sequences. The non-preservation probably occurs due to the small accommodation space, high wave energy and small sediment supply when compared to continental shelves. When sea level drops below its present level, sediment supply becomes sparse due to a lack of major river systems, reduced precipitation in colder periods and more limited subaerial erosion of the then moribund marine cliffs. Consequently, during sea level falls, sediment supply does not produce lowstand deposits. Furthermore, the narrow and steep insular margin and high wave energy may enhance transport of sediment offshore, with regressive ravinements removing the previous highstand deposits, leaving the shelf devoid of sediments. During the subsequent sea level rise, transgressive deposits are unlikely to accumulate substantially as the shelf would be sediment-starved because the only available sediment supply would be from a highstand palaeo-shore line. Not surprisingly, *Ávila et al.* [2008] relate the disappearance around 60 ka of (almost) all shallow bivalve species associated with sandy habitats on the Azorean islands to a starved shelf during a sea level drop.

[47] The efficient removal of older deposits found here, then raises the question of how shelf deposits can be preserved on some islands after passing through the surf zone, in particular, in the adjacent Azorean island Sta. Maria [*Serralheiro and Madeira*, 1993] and the Canary [*Zazo et al.*, 2002] and Cape Verde archipelagos [*Ramalho*, 2011; *Ramalho et al.*, 2010a; *Zazo et al.*, 2007, 2010]. Shelf sediments, now exposed subaerially on these islands, can only have been preserved during uplift if the sediment became armoured against erosion (e.g., calcite cements or from overlying lava flows as recorded around Hawai'i [*Lipman and Moore*, 1996; *Moore et al.*, 1996]) or if particular physiographies of

the shelf helped to dissipate wave energy (sheltering effect of nearby islands or wide, shallow shelves or banks).

5.5. Mass-Wasting Processes Around the Shelf Edge

[48] Headwall embayements and gullying have been found at the shelf edge of Faial. Gullying is frequent along the slopes of sectors A1 and A2 while around other sectors embayments are the most common features. Some of the possible causes for the initiation of submarine landslides, likely to have created these features, include oversteepening, seismic loading, storm-wave loading and incohesive nature of the sediments [*Hampton et al.*, 1996; *Locat and Lee*, 2002]. The shelf of Faial has the ideal physical conditions (high wave energy and narrow shelf) for the accumulation of material near the shelf break and shows evidence of sediment moving offshore (the highest thicknesses of the clinoform deposits are on the middle to the outer shelf) and possible spillover. Furthermore, the shelf is often struck by severe storms [*Andrade et al.*, 2008] and, on average, an earthquake occurs with $M_s > 6.5$ every 70 years [*Nunes et al.*, 2004]. It appears that the combination of abundant earthquakes, highly energetic wave environment, steep gradients on the shelf edge and accumulation of incohesive sediments are likely explanations for the mass-wasting in the areas that show embayments. Gullying is present in areas where the shelf edge is rocky, mostly from recent lava progradation. Probably the interaction of lava and sea swell [*Moore et al.*, 1973] has favored the development of extensive hyaloclastite deposits on the shelf edge which in turn were susceptible to slope failure.

5.6. Shelf Hydraulic Regime

[49] According to *Johnson and Baldwin* [1986] wave-dominated shelves are those characterized by seasonally fluctuating high wave and current intensity, with active sediment transport restricted to intermittent storms, where moderately grained sediments and small-scale bedforms predominate. Storm-dominated shelves are struck by high intensity and moderate/high frequency hurricane and tropical storms, where larger bedforms and coarse-grained sediments dominate. The shelf of Faial may be classified as wave-dominated shelf according to its sedimentary facies. No large bedforms are present on the shelf, except in the Faial-Pico inter-island channel which may be related to the strong tidal currents [*Tempera*, 2008]. Although storms are frequent in the Azores, the width of the shelf covered with sediments is very small, on average less than 1 km, not favoring the generation of large bedforms. The sedimentary cover is coarse-grained, although the lack of fine-grained sediments may also be a consequence of the limited fluvial sources. Nevertheless, the particle size is usually a good measure of the average kinetic energy of the depositing agent [*Greenwood*, 1969] and the importance of storm influences is corroborated by the instrumental and historical records of high energetic events [*Andrade et al.*, 2008; *Carvalho*, 2003; *Instituto Hidrográfico*, 2005]. Therefore, the above suggests that the shelf of Faial is wave- to-storm dominated.

5.7. Tectonics

[50] Our earlier erosion numerical simulation revealed differences between model and observed shelf break depths on Faial Island [see *Quartau et al.*, 2010, Table 2]. For instance, the average depth of the shelf break in sectors B, D, G and H are significantly different than −130 m. As we know, the shelf break is formed by wave erosion at, or close to, the water surface [*Trenhaile*, 2000, 2001] during low sea level and in the last 580 Ma, the lowest sea level was always around −130 m [*Bintanja et al.*, 2005]. Although small differences between model and data could merely reflect measurement or interpretation errors in the field or inaccurate palaeo-sea level data, the differences that are more significant are better explained by other processes. The tectonic structure of the island is a graben (Figures 2a and 2c), so the central part of it (extending from the Faial-Pico channel on the east to the NW littoral - sector B) should record the highest subsidence; on the other hand, the north and south coasts should be uplifted. All of this agrees well with the values from Table 2 of *Quartau et al.* [2010]; sectors G and H show uplift and sector B subsidence. Sector D should also show uplift, but instead its shelf break is at −211 m which could only be explained by subsidence due to the built-up of the central Caldeira volcano on the western flank of the Ribeirinha Volcano. In a similar way, we should expect the same amount of subsidence for sector F, however its shelf break is at −127 m. Nevertheless, this sector was formed during the stage of renewed volcanism from the Almoxarife Formation which may have filled a depressed shelf and elevated the shelf break (example i_d in Figure 14). The graben faults also provided

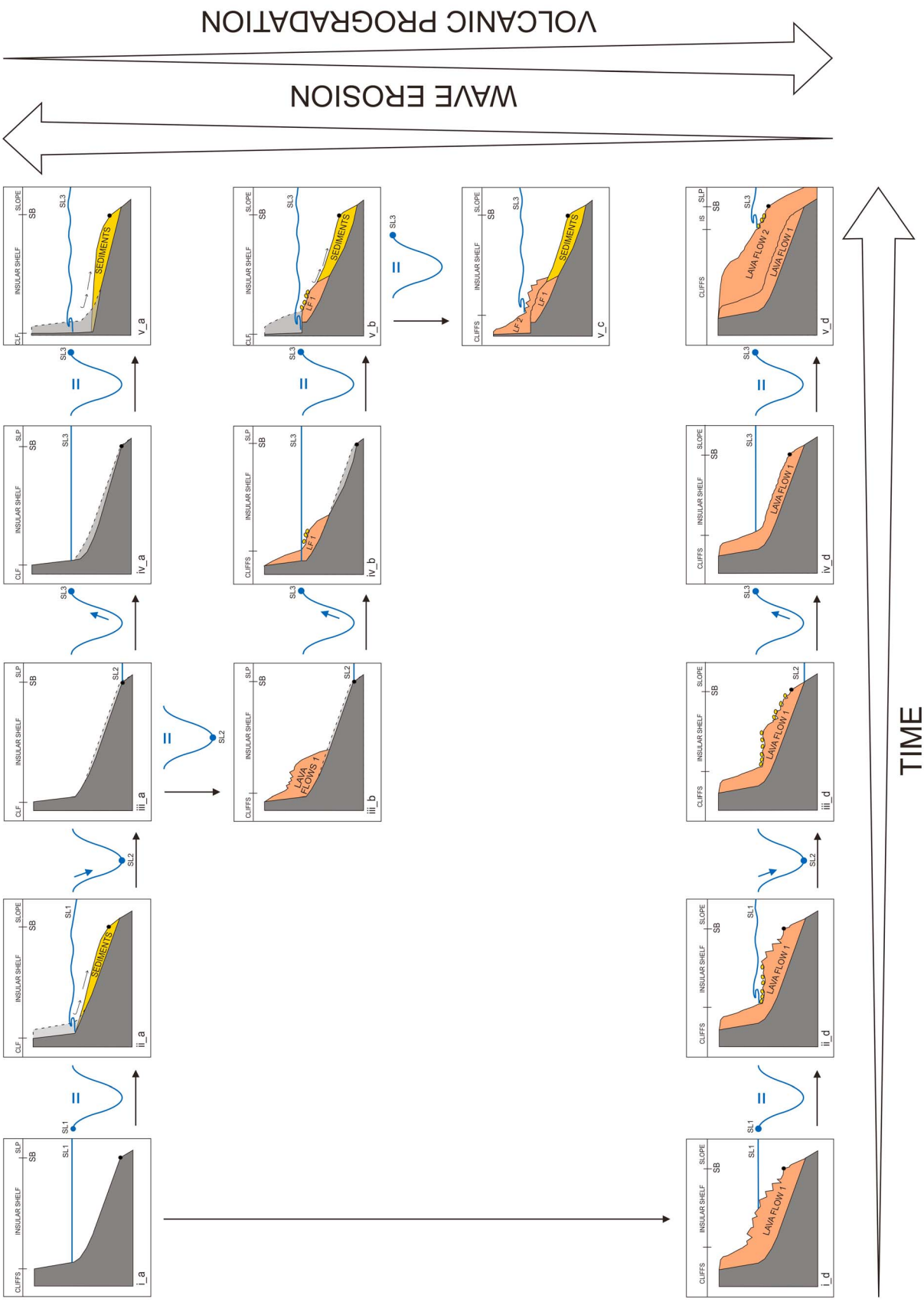
VOLCANIC PROGRADATION
WAVE EROSION
TIME
i_a
ii_a
iii_a
iv_a
v_a
iii_b
iv_b
v_b
v_c
i_d
ii_d
iii_d
iv_d
v_d
INSULAR SHELF
CLIFFS
SLOPE
SB
SLP
IS
CLF
SL1
SL2
SL3
SEDIMENTS
LAVA FLOWS 1
LAVA FLOW 1
LAVA FLOW 2
LF 1
LF 2

Figure 14

weaknesses exploited by streams in the coastline of sector B and mass-wasting in the shelf edge (Figure 12), although their shelf connection is difficult to observe due to the sedimentary cover and lack of seismic data here. The faults also control the drainage in the east of Faial (Figure 2c), modifying the radial drainage around Caldeira volcano and thus deviating sediments that would otherwise feed shelf sectors C, D, F and G to the inter-island channel Faial-Pico (sector E).

5.8. Conceptual Model of the Morphologic Development of the Faial shelf

[51] Based on our results, a conceptual model of the development of the Faial shelf is proposed (Figure 14). Although it is simplified by not including subaerial (explosive volcanism and stream erosion) tectonic and mass-wasting processes, it includes the two main processes (wave erosion and volcanic progradation) responsible for its evolution. The sketch starts with a volcanic island shelf formed by wave erosion during one or more glacial–interglacial sea level oscillations (i_a). From this initial stage with sea level at a highstand position (SL1), the shelf has developed into the four end-member stages (v_a, v_b, v_c and v_d):

[52] 1. From i_a to v_a. If volcanism has stopped or is too small to reach the coastline, wave erosion starts eroding cliffs, producing sediments nearshore which are then redistributed over the shelf by downwelling currents formed during storms (ii_a). When sea level drops, since the main supply of sediments to the shelf are left behind (cliffs), there is no significant sediment production and the previous highstand body is swept from the shelf by downwelling currents, until it is ultimately lost during the lowstand (SL2) to the island slope (iii_a). At the same time during this sea level fall a small abrasion of the shelf occurs. When sea level starts to rise, the shelf is eroded again, but not sufficiently to build and maintain a sedimentary body (iv_a). When sea level reaches a highstand position again (SL3), cliffs start to retreat and considerable amount of sediment is produced nearshore, the shelf widens and the sedimentary deposits start to form, thicker than before due to the higher accommodation space (v_a). Eventually, if the shelf widens sufficiently to attenuate wave energy during the following sea level oscillations, older depositional sequences and systems tracts associated with sea level changes normally described for continental shelves can be preserved.

[53] 2. From i_a to v_b, with shared evolution from i_a to iii_a. During iii_a, if volcanic activity (lava flow 1 - LF1) is strong enough to move the coastline to the inner shelf, the shelf width is reduced (iii_b). When sea level rises again, it erodes shallowly the entire shelf probably depositing thin transgressive sediments. However, those formed on top of the prograded lava flows (iv_b) are too coarse to be swept way by downwelling currents, but the ones below probably are, hence, they are not preserved at this stage. Only when sea level reaches SL3, a sedimentary body starts to grow on the mid-shelf by erosion of the nearshore deposits of LF1 and the cliff. The sediments produced are then redistributed through downwellling currents formed during storms, filling the mid to outer shelf (v_b).

[54] 3. From i_a to v_c with shared evolution until v_b. Renewed volcanic activity (v_c) moves again the coastline offshore with a new lava flow (LF2) on top of the previous one (LF1) which, if it is voluminous enough, it may even bury part of the sedimentary body.

[55] 4. From i_a to v_d. If volcanism is very voluminous, it can cover the entire shelf and move the previous coastline to the middle shelf (i_d). Wave erosion during stable sea level SL1 is able to carve a platform on top of the prograded lava flow forming a cover of coarse clastic deposits on top of it (ii_d). When sea level drops to SL2, the entire prograded volcanics are abraded to the shelf break, leaving behind a cover of coarse clastic deposits (iii_d). When sea level rises again, it further carves the prograded volcanics, reducing the coarse clastics to sandy sediments, which are probably not

Figure 14. Conceptual model of the morphologic development of the Faial shelf. Each square represents a cross-shore profile of the shelf with very high vertical exaggeration. The model starts at i_a and develops into the four possible stages v_a, v_b, v_c and v_d. Inside the squares, gray dark areas represent the cliff (CLF), the insular shelf (IS) and the upper slope (SLP) of a coastal sector of the island, light gray represents erosion within those areas, yellow areas represent sandy sedimentary deposits, the orange areas preserved or eroded lava flows, blue lines represent sea level and black dots represent the shelf edge. Between the squares blue curves represent sea level oscillations; blue dots position of sea level inside the curve, blue arrows the direction of sea level and equal signal stable sea level. Black horizontal and vertical arrows represent time evolution. From top to bottom is represented the decreasing contribution of wave erosion and increasing contribution of volcanic progradation processes.

volumetric enough to form sedimentary bodies (iv_d). If volcanic activity continues immediately after reaching SL3, there is no time to build a sedimentary body and the coastline is moved again offshore, further reducing the shelf width (v_d).

[56] All these examples can be found on Faial's shelf with predominance of stage v_d on the more volcanic active and young sectors (sectors A1 and A2) and v_c, v_b and v_a progressively on less active and older sectors. Although this model is put forward to explain the development of the various sectors of Faial's shelf, we suggest that it is likely to apply also to other volcanic island shelves in oceanographic settings unfavorable to reef growth where wave erosion and volcanic progradation are the main generating processes.

6. Conclusions

[57] The combined use of multibeam bathymetry and acoustic backscattering, chirp bottom echo character, seismic stratigraphy, superficial sediment sampling and seafloor images permitted the mapping and description of the seabed morphologies around Faial's shelf, providing clues to the relative roles of the various processes involved in its development:

[58] 1. The shelf is the result of wave erosion evidenced by a platform extending hundreds to thousands of meters from the coastline to the shelf edge. Shelf width is related to shelf age and wave energy exposure. The study of the shelf morphology in young volcanic islands where erosion dominates can help to constrain the chronology of onshore volcanic emplacements, especially when reliable dates are not available.

[59] 2. Seaward volcanic progradation can reverse the onshore coastline retreat by filling the shelf created by erosion. Nevertheless, we have found fewer submarine-emplaced lavas on the shelf when compared to nearby Pico, which is a sign of Faial's maturity.

[60] 3. Sandy clinoforms have been deposited over the volcanic platform of Faial during the last 6.5 ka by storm-induced downwelling currents that transport sediment offshore. In other volcanic islands (Oahu and the Aeolian archipelago) the same mechanism has been invoked to explain their shelf deposits. The lack of preservation of older deposits associated with previous sea level changes in volcanic insular shelves is due to the presence of narrow and steep shelves, high wave energy, and low sediment supply. However, during uplift older deposits can be preserved if the sediment is armoured against surf erosion or waves are reduced by local physiography (e.g., Azores, Canary and Cape Verde archipelagos).

[61] 4. The shelf sediments around Faial are mostly volcaniclastic and result mainly from cliff erosion, with lesser contributions from subaerial erosion and explosive volcanism. The area and thickness of the deposits are related to wave exposure, with larger deposits normally found on the more wave-energetic sectors and with greater accommodation space.

[62] 5. Mass-wasting at the shelf edge is suggested to be the result of frequent earthquakes, high-wave energy associated with storms, over-steepening of incohesive sediments and their possible spillover near the shelf edge. In areas where sediments reach the shelf edge, slides are common; whereas in areas where the shelf edge is rocky, gullies prevail.

[63] 6. The shelf of Faial can be classified as wave to storm-dominated according to *Johnson and Baldwin*'s [1986] classification.

[64] 7. Movement on tectonic faults has changed the depth of the erosional shelf edge in some sectors, and consequently changed the accommodation space available. It might have also promoted canyon incision in the west and sediment accumulation in the east.

[65] A conceptual model of the morphologic development of the Faial shelf is proposed based on the main processes acting on the shelf; wave erosion and volcanic progradation. We expect that these results may contribute to a better understanding of the processes involved in the development of other reefless volcanic island shelves.

Acknowledgments

[66] Seismic acquisition and sediment sampling in the shelf of Faial was conducted in the scope of the GEMAS Project funded by Secretaria Regional do Ambiente dos Açores and our project partner, the Departamento de Oceanografia e Pescas da Universidade dos Açores. The following agencies are gratefully acknowledged for providing funding toward the multibeam survey: the Royal Society, the British Council, the Higher Education Funding Council for Wales, the Regional Directorate for Science and Technology of the Azores and Portuguese projects MARINOVA (INTERREG IIIb/MAC/4.2/M11), MAROV (PDCTM/P/MAR/15249/1999), MAYA (AdI/POSI/2003) and MeshAtlantic (AA-10/1218525/BF). IMAR-DOP/UAz is Research and Development Unit no. 531 and LARSyS-Associated Laboratory no. 9 funded by the Portuguese

Foundation for Science and Technology (FCT) by the Azores Directorate for Science and Technology (DRCT) through funding schemes (FEDER, POCI2001, FSE, COMPETE and project PEst-OE/EEI/LA0009/2011). R.Q. was funded by a postdoctoral fellowship (SFRH/BPD/27135/2006) and F.T. through a Ph.D. grant (SFRH/BD/12885/2003), both from the Fundação para a Ciência e Tecnologia. Part of this work was also possible through the support of the INGMAR project financed by Laboratório Nacional de Energia e Geologia (LNEG). The authors and the LNEG also acknowledge the support by Landmark Graphics Corporation via the Landmark University Grant Program, and CARIS, Inc. for the CARIS HIPS & SIPS license granted under the academic agreement with IMAR-Instituto do Mar (Ref.: 2009-02-APP08). The Estrutura de Missão para a Extensão da Plataforma Continental (EMEPC) is acknowledged for the acquisition, processing and sharing of multibeam data covering parts of Faial island shelf break. The first author also acknowledges helpful discussions with Cristina Roque (LNEG), Ricardo Ramalho (Department of earth Sciences, University of Bristol) and Claudia Romagnoli (Dipartimento di Scienze della Terra e Geologico-ambientali, Università di Bologna). Constructive reviews by José Madeira and John R. Smith helped to significantly improve the manuscript.

References

Ablay, G., and M. Hurlimann (2000), Evolution of the north flank of Tenerife by recurrent giant landslides, *J. Volcanol. Geotherm. Res.*, *103*, 135–159, doi:10.1016/S0377-0273(00)00220-1.

Andrade, C., R. M. Trigo, M. C. Freitas, M. C. Gallego, P. Borges, and A. M. Ramos (2008), Comparing historic records of storm frequency and the North Atlantic Oscillation (NAO) chronology for the Azores region, *Holocene*, *18*(5), 745–754, doi:10.1177/0959683608091794.

Ávila, S. P., P. Madeira, C. Marques da Silva, M. Cachão, R. Quartau, B. Landau, and A. M. F. Martins (2008), Local disappearance of bivalves in the Azores during the last glaciation, *J. Quat. Sci.*, *23*(8), 777–785, doi:10.1002/jqs.1165.

Bintanja, R., R. S. W. van de Wal, and J. Oerlemans (2005), Modelled atmospheric temperatures and global sea levels over the past million years, *Nature*, *437*(7055), 125–128, doi:10.1038/nature03975.

Borges, P. (2003), Ambientes litorais nos Grupos Central e Oriental do arquipélago dos Açores, PhD thesis, Dep. Geociências, Univ. dos Açores, Ponta Delgada, Portugal.

Carracedo, J. C. (1999), Growth, structure, instability and collapse of Canarian volcanoes and comparisons with Hawaiian volcanoes, *J. Volcanol. Geotherm. Res.*, *94*(1–4), 1–19, doi:10.1016/S0377-0273(99)00095-5.

Carvalho, F. (2002), Apuramentos climatológicos mensais em Açores central no período 1989–2002, report, Inst. de Meteorol., Lisboa.

Carvalho, F. (2003), Elementos do clima de agitação marítima no grupo central dos Açores, report, Inst. de Meteorol., Lisboa.

Catuneanu, O. (2002), Sequence stratigraphy of clastic systems: Concepts, merits, and pitfalls, *J. Afr. Earth Sci.*, *35*, 1–43, doi:10.1016/S0899-5362(02)00004-0.

Chiocci, F. L., and C. Romagnoli (2004), Submerged depositional terraces in the Aeolian Islands (Sicily), in *Atlas of Submerged Depositional Terraces Along the Italian Coasts*, *Mem. Descr. Carta Geol. Ital.*, edited by F. L. Chiocci, S. D'Angelo, and C. Romagnoli, pp. 81–114, APAT, Rome.

Chovelon, P. (1982), Évolution volcanotectonique des iles de Faial et de Pico, Archipel des Açores - Atlantique Nord, PhD thesis, Univ. de Paris-Sud, Paris, France.

Cole, P. D., J. E. Guest, and A. M. Duncan (1996), Capelinhos: The disappearing volcano, *Geol. Today*, *12*, 68–72, doi:10.1046/j.1365-2451.1996.00010.x.

Cole, P. D., J. E. Guest, A. M. Duncan, and J.-M. Pacheco (2001), Capelinhos 1957–1958, Faial, Azores: Deposits formed by an emergent surtseyan eruption, *Bull. Volcanol.*, *63*, 204–220, doi:10.1007/s004450100136.

Collier, J. S., and A. B. Watts (2001), Lithospheric response to volcanic loading by the Canary Islands: Constraints from seismic reflection data in their flexural moat, *Geophys. J. Int.*, *147*(3), 660–676, doi:10.1046/j.0956-540x.2001.01506.x.

Coulbourn, W. T., J. F. Campbell, and R. Moberly (1974), Hawaiian submarine terraces, canyons and quaternary history evaluated by seismic-reflection profiling, *Mar. Geol.*, *17*, 215–234, doi:10.1016/0025-3227(74)90073-5.

Dabrio, C. J., C. Zazo, J. L. Goy, F. J. Sierro, F. Borja, J. Lario, J. A. González, and J. A. Flores (2000), Depositional history of estuarine infill during the last postglacial transgression (Gulf of Cadiz, Southern Spain), *Mar. Geol.*, *162*(2–4), 381–404, doi:10.1016/S0025-3227(99)00069-9.

Damuth, J. E. (1975), Echo character of the Western Equatorial Atlantic floor and its relationship to the dispersal distribution of terrigenous sediments, *Mar. Geol.*, *18*, 17–45, doi:10.1016/0025-3227(75)90047-X.

Damuth, J. E. (1980), Use of high-frequency (3.5–12kHz) echograms in the study of near-bottom sedimentation processes in the deep-sea: A review, *Mar. Geol.*, *38*, 51–75, doi:10.1016/0025-3227(80)90051-1.

Damuth, J. E., and D. E. Hayes (1977), Echo character of the east Brazilian continental margin and its relationship to sedimentary processes, *Mar. Geol.*, *24*, 73–95, doi:10.1016/0025-3227(77)90002-0.

Dickson, M. E. (2004), The development of talus slopes around Lord Howe island and implications for the history of island planation, *Aust. Geogr.*, *35*, 223–238, doi:10.1080/0004918042000249520.

DROTRH-IA (2001), Plano regional da água - Relatório técnico - Versão para consulta pública, Ed. Secretaria Regional do Ambiente, Direcção Regional do Ordenamento do Território e dos Recursos Hídricos, technical report, Ponta Delgada, Portugal.

Favalli, M., D. Karátson, R. Mazzuoli, M. Pareschi, and G. Ventura (2005), Volcanic geomorphology and tectonics of the Aeolian archipelago (Southern Italy) based on integrated DEM data, *Bull. Volcanol.*, *68*(2), 157–170, doi:10.1007/s00445-005-0429-3.

Féraud, G. (1980), Contribution à la datation du volcanisme de l'archipel des Açores par la méthode Potassium-Argon. Conséquences géodynamiques, PhD thesis, 186 pp., Univ. de Paris-Sud, Paris.

Féraud, G., I. Kaneoka, and C. J. Allègre (1980), K-Ar ages and stress pattern in the Azores: Geodynamic implications, *Earth Planet. Sci. Lett.*, *46*(2), 275–286, doi:10.1016/0012-821X(80)90013-8.

Ferreira, D. B. (1981), Les méchanismes des pluies et les types de temps de saisons fraiches aux Açores, *Finisterra*, *16*(31), 15–61.

Field, M. E., and P. S. Roy (1984), Offshore transport and sand-body formation; evidence from a steep, high energy

shoreface, southeastern Australia, *J. Sediment. Res.*, *54*, 1292–1302.
Forjaz, V. H. (2004), *Atlas Básico dos Açores*, Obs. Vulcanológico e Geotérmico dos Açores, Ponta Delgada, Portugal.
Garcia, M. O., and M. G. Davis (2001), Submarine growth and internal structure of ocean island volcanoes based on submarine observations of Mauna Loa volcano, Hawaii, *Geology*, *29*(2), 163–166, doi:10.1130/0091-7613(2001)029<0163:SGAISO>2.0.CO;2.
Greenwood, B. (1969), Sediment parameters and environment discrimination: An application of multivariate statistics, *Can. J. Earth Sci.*, *6*, 1347–1358.
Grossman, E. E., W. A. Barnhardt, P. Hart, B. M. Richmond, and M. E. Field (2006), Shelf stratigraphy and the influence of antecedent substrate on Holocene reef development, south Oahu, Hawaii, *Mar. Geol.*, *226*(1–2), 97–114, doi:10.1016/j.margeo.2005.09.012.
Hamilton, E. L., and R. T. Bachman (1982), Sound velocity and related properties in marine sediments, *J. Acoust. Soc. Am.*, *72*(6), 1891–1904, doi:10.1121/1.388539.
Hampton, M. A., H. J. Lee, and J. Locat (1996), Submarine landslides, *Rev. Geophys.*, *34*, 33–59, doi:10.1029/95RG03287.
Hampton, M. A., C. T. Blay, and C. J. Murray (2004), Carbonate sediment deposits on the reef front around Oahu, Hawaii, *Mar. Georesour. Geotechnol.*, *22*, 65–102, doi:10.1080/10641190490473407.
Hernández-Molina, F. J., L. Somoza, J. Rey, and L. Pomar (1994), Late Pleistocene-Holocene sediments on the Spanish continental shelves: Model for very high resolution sequence stratigraphy, *Mar. Geol.*, *120*(3–4), 129–174, doi:10.1016/0025-3227(94)90057-4.
Hernández-Molina, F. J., L. M. Fernández-Salas, F. Lobo, L. Somoza, V. Díaz-del-Río, and J. M. Alveirinho Dias (2000), The infralittoral prograding wedge: A new large-scale progradational sedimentary body in shallow marine environments, *Geo Mar. Lett.*, *20*(2), 109–117, doi:10.1007/s003670000040.
Instituto Geográfico do Exército (2001a), Portuguese military map, sheet 4, Praia do Norte (Faial-Açores), scale 1:25,0000, Lisboa.
Instituto Geográfico do Exército (2001b), Portuguese military map, sheet 5, Pedro Miguel (Faial-Açores), scale 1:25,0000, Lisboa.
Instituto Geográfico do Exército (2001c), Portuguese military map, sheet 6, Feteira (Faial-Açores), scale 1:25,0000, Lisboa.
Instituto Geográfico do Exército (2001d), Portuguese military map, sheet 7, Horta (Faial-Açores), scale 1:25,0000, Lisboa.
Instituto Hidrográfico (Ed.) (2000), *Arquipélago dos Açores*, 2nd ed., Lisboa.
Instituto Hidrográfico (2005), Tratamentos de dados de agitação maritime, Açores/Terceira - Fevereiro 2005, report, Lisboa.
Intergovernmental Oceanographic Commission, International Hydrographic Organization, and British Oceanographic Data Centre (2003), *Centenary Edition of the GEBCO Digital Atlas* [CD-ROM], Br. Oceanogr. Data Cent., Liverpool, U. K.
Johnson, H. D., and C. T. Baldwin (1986), Shallow siliclastic seas, in *Sedimentary Environments and Facies*, edited by H. G. Reading, pp. 229–282, Blackwell Sci., Oxford, U. K.
Krause, D. C., and N. D. Watkins (1970), North Atlantic crustal genesis in the vicinity of the Azores, *Geophys. J. R. Astron. Soc.*, *19*, 261–283, doi:10.1111/j.1365-246X.1970.tb06046.x.
Laughton, A. S., and R. B. Whitmarsh (1974), The Azores-Gibraltar plate boundary, in *Geodynamics of Iceland and the North Atlantic Area*, edited by L. Kristjansson, pp. 63–81, Reidel, Dordrecht, Netherlands.
Le Friant, A., C. L. Harford, C. Deplus, G. Boudon, R. J. S. Sparks, R. A. Herd, and J.-C. Komorowski (2004), Geomorphological evolution of Monserrat (West Indies): Importance of flank collapse and erosional processes, *J. Geol. Soc.*, *161*, 147–160, doi:10.1144/0016-764903-017.
Lipman, P. W., and J. G. Moore (1996), Mauna Loa lava accumulation rates at the Hilo drill site: Formation of lava deltas during a period of declining overall volcanic growth, *J. Geophys. Res.*, *101*(B5), 11,631–11,641, doi:10.1029/95JB03214.
Llanes, P., R. Herrera, M. Gómez, A. Muñoz, J. Acosta, E. Uchupi, and D. Smith (2009), Geological evolution of the volcanic island La Gomera, Canary Islands, from analysis of its geomorphology, *Mar. Geol.*, *264*(3–4), 123–139, doi:10.1016/j.margeo.2009.05.001.
Locat, J., and H. J. Lee (2002), Submarine landslides: Advances and challenges, *Can. Geotech. J.*, *39*(1), 193–212, doi:10.1139/t01-089.
Lourenço, N., J. M. Miranda, J. F. Luís, A. Ribeiro, L. A. Mendes Victor, J. Madeira, and H. D. Needham (1998), Morpho-tectonic analysis of the Azores Volcanic Plateau from a new bathymetric compilation of the area, *Mar. Geophys. Res.*, *20*(3), 141–156, doi:10.1023/A:1004505401547.
Louvat, P., and C. J. Allègre (1998), Riverine erosion rates on São Miguel volcanic island, Azores archipelago, *Chem. Geol.*, *148*, 177–200, doi:10.1016/S0009-2541(98)00028-X.
Madeira, J. (1998), Estudos de neotectónica nas ilhas do Faial, Pico e S. Jorge: Uma contribuição para o conhecimento geodinâmico da junção tripla dos Açores, PhD thesis, Dep. de Geologia, Univ. de Lisboa, Lisboa.
Madeira, J., and A. Brum da Silveira (2003), Active tectonics and first paleosismological results in Faial, Pico e S. Jorge islands (Azores, Portugal), *Ann. Geophys.*, *46*(5), 733–761.
Madeira, J., A. M. M. Soares, A. Brum da Silveira, and A. Serralheiro (1995), Radiocarbon dating recent volcanic activity on Faial Island (Azores), *Radiocarbon*, *37*(2), 139–147.
Masson, D. G., T. P. Le Bas, I. Grevemeyer, and W. Weinrebe (2008), Flank collapse and large-scale landsliding in the Cape Verde Islands, off West Africa, *Geochem. Geophys. Geosyst.*, *9*, Q07015, doi:10.1029/2008GC001983.
Mattox, T. N., and M. T. Manga (1997), Littoral hydrovolcanic explosions: A case study of lava-seawater interaction at Kilauea Volcano, *J. Volcanol. Geotherm. Res.*, *75*, 1–17, doi:10.1016/S0377-0273(96)00048-0.
McMurtry, G. M., P. Watts, G. J. Fryer, J. R. Smith, and F. Imamura (2004), Giant landslides, mega-tsunamis, and paleo-sea level in the Hawaiian Islands, *Mar. Geol.*, *203*(3–4), 219–233, doi:10.1016/S0025-3227(03)00306-2.
Menard, H. W. (1983), Insular erosion, isostasy, and subsidence, *Science*, *220*, 913–918, doi:10.1126/science.220.4600.913.
Menard, H. W. (1984), Origin of guyots: The Beagle to Seabeam, *J. Geophys. Res.*, *89*, 11,117–11,123, doi:10.1029/JB089iB13p11117.
Menard, H. W. (1986), *Islands*, Sci. Am. Books, New York.
Mitchell, N. C. (2003), Susceptibility of mid-ocean ridge volcanic islands and seamounts to large-scale landsliding, *J. Geophys. Res.*, *108*(B8), 2397, doi:10.1029/2002JB001997.

Mitchell, N. C., M. A. Tivey, and P. Gente (2000), Seafloor slopes at mid-ocean ridges from submersible observations and implications for interpreting geology from seafloor topography, *Earth Planet. Sci. Lett.*, *183*, 543–555, doi:10.1016/S0012-821X(00)00270-3.

Mitchell, N. C., D. G. Masson, A. B. Watts, M. J. R. Gee, and R. Urgeles (2002), The morphology of the flanks of volcanic ocean islands: A comparative study of the Canary and Hawaiian hotspot islands, *J. Volcanol. Geotherm. Res.*, *115*, 83–107, doi:10.1016/S0377-0273(01)00310-9.

Mitchell, N. C., W. B. Dade, and D. G. Masson (2003a), Erosion of the submarine flanks of the Canary Islands, *J. Geophys. Res.*, *108*(F1), 6002, doi:10.1029/2002JF000003.

Mitchell, N. C., T. Schmidt, E. Isidro, F. Tempera, F. Cardigos, J. C. Nunes, and J. Figueiredo (2003b), Multibeam sonar survey of the central Azores volcanic islands, *InterRidge News*, *12*(2), 30–32.

Mitchell, N. C., C. Beier, P. Rosin, R. Quartau, and F. Tempera (2008), Lava penetrating water: Submarine lava flows around the coasts of Pico Island, Azores, *Geochem. Geophys. Geosyst.*, *9*, Q03024, doi:10.1029/2007GC001725.

Mitchell, N. C., R. Quartau, and J. Madeira (2012), Assessing landslide movements in volcanic islands using near-shore marine geophysical data: South Pico island, Azores, *Bull. Volcanol.*, *74*, 483–496, doi:10.1007/s00445-011-0541-5.

Mitchum, R. M., Jr., P. R. Vail, and J. B. Sangree (1977a), Seismic stratigraphy and global changes in sea level, Part 6: Stratigraphic interpretation of seismic reflection patterns in depositional sequences, in *Seismic Stratigraphy–Applications to Hydrocarbon Exploration*, edited by C. E. Payton, *AAPG Mem.*, *26*, 117–133.

Mitchum, R. M., Jr., P. R. Vail, and S. Thompson III (1977b), Seismic stratigraphy and global changes of sea level, Part 2: The depositional sequence as a basic unit for stratigraphic analysis, in *Seismic Stratigraphy–Applications to Hydrocarbon Exploration*, edited by C. E. Payton, *AAPG Mem.*, *26*, 53–62.

Moore, J. G., R. L. Philips, R. W. Grigg, D. W. Peterson, and D. A. Swanson (1973), Flow of lava into the sea, 1969–1971, Kilauea volcano, Hawaii, *Geol. Soc. Am. Bull.*, *84*, 537–546, doi:10.1130/0016-7606(1973)84<537:FOLITS>2.0.CO;2.

Moore, J. G., W. R. Normark, and R. T. Holcomb (1994), Giant Hawaiian landslides, *Annu. Rev. Earth Planet. Sci.*, *22*(1), 119–144, doi:10.1146/annurev.ea.22.050194.001003.

Moore, J. G., B. L. Ingram, K. R. Ludwig, and D. A. Clague (1996), Coral ages and island subsidence, Hilo drill hole, *J. Geophys. Res.*, *101*(B5), 11,599–11,605, doi:10.1029/95JB03215.

Morelock, J., K. Grove, and M. L. Hernandez (1983), Oceanography and patterns of shelf sediments, Mayaguez, Puerto Rico, *J. Sediment. Res.*, *53*(2), 371–381.

Müller, G., and M. Gastner (1971), The "Karbonate Bombe"; A simple device for the determination of the carbonate content in sediments, soils and other materials, *Neues Jahrb. Mineral.*, *10*, 466–469.

Nittrouer, C. A., and L. D. Wright (1994), Transport of particles across continental shelves, *Rev. Geophys.*, *32*, 85–113, doi:10.1029/93RG02603.

Nunes, J. C., V. H. Forjaz, and C. S. Oliveira (2004), Catálogo sísmico da região dos Açores (1850–1998), paper presented at 6th Congresso Nacional de Sismologia e Engenharia Sísmica, Univ. do Minho, Braga, Portugal.

Oehler, J.-F., J.-F. Lénat, and P. Labazuy (2008), Growth and collapse of the Reunion Island volcanoes, *Bull. Volcanol.*, *70*(6), 717–742, doi:10.1007/s00445-007-0163-0.

Pacheco, J. M. (2001), Processos associados ao desenvolvimento de erupções vulcânicas hidromagmáticas explosivas na ilha do Faial e sua interpretação numa perspectiva de avaliação do Hazard e minimização de risco, PhD thesis, Dep. de Geociências, Univ. dos Açores, Ponta Delgada, Portugal.

Paduan, J. B., D. A. Clague, and A. S. Davis (2009), Evidence that three seamounts off southern California were ancient islands, *Mar. Geol.*, *265*(3–4), 146–156, doi:10.1016/j.margeo.2009.07.003.

Powers, M. C. (1953), A new roundness scale for sedimentary particles, *J. Sediment. Petrol.*, *23*(2), 117–119.

Pratson, L. F., and E. P. Laine (1989), The relative importance of gravity induced versus current-controled sedimentation during the Quaternary along the mideast US outer continental margin revealed by 3.5 kHz echo character, *Mar. Geol.*, *89*, 87–126, doi:10.1016/0025-3227(89)90029-7.

Quartau, R. (2007), The insular shelf of Faial: Morphological and sedimentary evolution, PhD thesis, Dep. de Geociências. Univ. de Aveiro, Aveiro, Portugal.

Quartau, R., F. Curado, T. Cunha, L. Pinheiro, and J. H. Monteiro (2002), Projecto Gemas–Localização e distribuição de areias em redor da ilha do Faial, *Tech. Rep. INGMARDEP 5/2002*, Dep. Geol. Mar.-IGM, Lisboa.

Quartau, R., H. Duarte, and P. Brito (2005), Projecto Gemas–Relatório da campanha de amostragem de sedimentos (FAPI-3) realizada na plataforma e na orla costeira das ilhas do Faial e do Pico, *Tech. Rep. INGMARDEP 2/2005*, Dep. Geol. Mar.-INETI, Lisboa.

Quartau, R., A. S. Trenhaile, N. C. Mitchell, and F. Tempera (2010), Development of volcanic insular shelves: Insights from observations and modelling of Faial Island in the Azores Archipelago, *Mar. Geol.*, *275*(1–4), 66–83, doi:10.1016/j.margeo.2010.04.008.

Quidelleur, X., A. Hildenbrand, and A. Samper (2008), Causal link between Quaternary paleoclimatic changes and volcanic islands evolution, *Geophys. Res. Lett.*, *35*, L02303, doi:10.1029/2007GL031849.

Ramalho, R. (2011), Building the Cape Verde Islands, PhD thesis, Univ. of Bristol, Bristol, U. K.

Ramalho, R., G. Helffrich, D. N. Schmidt, and D. Vance (2010a), Tracers of uplift and subsidence in the Cape Verde archipelago, *J. Geol. Soc.*, *167*(3), 519–538, doi:10.1144/0016-76492009-056.

Ramalho, R., G. Helffrich, M. Cosca, D. Vance, D. Hoffmann, and D. N. Schmidt (2010b), Episodic swell growth inferred from variable uplift of the Cape Verde hotspot islands, *Nat. Geosci.*, *3*(11), 774–777, doi:10.1038/ngeo982.

Santos, F. D., M. A. Valente, P. M. A. Miranda, A. Aguiar, E. B. Azevedo, A. R. Tomé, and F. Coelho (2004), Climate change scenarios in the Azores and Madeira Islands, *World Resour. Rev.*, *16*(4), 473–491.

Schmincke, H.-U. (2004), Seamounts and volcanic islands, in *Volcanism*, pp. 71–96, Springer, Berlin, doi:10.1007/978-3-642-18952-4_6.

Schneidermann, N., O. H. Pilkey, and C. Saunders (1976), Sedimentation on the Puerto Rico insular shelf, *J. Sediment. Res.*, *46*(1), 167–173.

Scott, G. A. J., and G. M. Rotondo (1983), A model to explain the differences between Pacific plate island-atoll types, *Coral Reefs*, *1*(3), 139–150, doi:10.1007/BF00571191.

Serralheiro, A., and J. Madeira (1993), Stratigraphy and geochronology of Santa Maria Island (Azores), *Açoreana*, *7*(4), 575–592.

Serralheiro, A., V. H. Forjaz, C. M. A. Alves, and B. Rodrigues (1989), Volcanological Map of the Azores – Faial Island,

scale 1:50,000, Serv. de Protecção Civ., Ponta Delgada, Portugal.

Staudigel, H., and D. A. Clague (2010), The geological history of deep-sea volcanoes: Biosphere, hydrosphere, and lithosphere interactions, *Oceanography*, *23*(1), 58–71, doi:10.5670/oceanog.2010.62.

Teixeira, F. C. (2001), Projecto Gemas–Relatório da campanha FAPI1–2001 realizada ao largo do Faial, *Tech. Rep. INGMARDEP 13/2001*, Dep. Geol. Mar.-IGM, Lisboa.

Tempera, F. (2008), Benthic habitats of the extended Faial Island shelf and their relationship to geologic, oceanographic and infralittoral biologic features, PhD thesis, Univ. of St. Andrews, St. Andrews, U. K.

Tempera, F., M. McKenzie, I. Bashmachnikov, M. Puotinen, R. S. Santos, and R. Bates (2012), Predictive modelling of dominant macroalgae abundance on temperate island shelves (Azores, northeast Atlantic), in *Seafloor Geomorphology as Benthic Habitat: Geohab Atlas of Seafloor Geomorphic Features and Benthic Habitats*, edited by E. Baker and P. Harris, pp. 169–184, Elsevier, London, doi:10.1016/B978-0-12-385140-6.00008-6.

Trenhaile, A. S. (2000), Modeling the development of wave-cut platforms, *Mar. Geol.*, *166*, 163–178, doi:10.1016/S0025-3227(00)00013-X.

Trenhaile, A. S. (2001), Modelling the Quaternary evolution of shore platforms and erosional continental shelves, *Earth Surf. Processes Landforms*, *26*, 1103–1128, doi:10.1002/esp.255.

U.S. Department of Defense (2001), Global Positioning System: Standard positioning service performance standard, report, Washington D. C.

Wentworth, C. K. (1922), A scale of grade and class terms for clastic systems, *J. Geol.*, *30*, 377–392, doi:10.1086/622910.

Wolfe, C. J., M. K. McNutt, and R. S. Detrick (1994), The Marquesas archipelagic apron: Seismic stratigraphy and implications for volcano growth, mass wasting, and underplating, *J. Geophys. Res.*, *99*, 13,591–13,608, doi:10.1029/94JB00686.

Youssef, W. B. H. (2005), Caractérisation *in situ* de l'environnement physique des habitats benthiques occupés par *Codium elisabethae* au sein de sites d'études particuliers (Faial, Açores), M.S. thesis, Univ. de Liège, Liège, France.

Zazo, C., J. L. Goy, C. Hillaire-Marcel, P.-Y. Gillot, V. Soler, J. Á. González, C. J. Dabrio, and B. Ghaleb (2002), Raised marine sequences of Lanzarote and Fuerteventura revisited-a reappraisal of relative sea level changes and vertical movements in the eastern Canary Islands during the Quaternary, *Quat. Sci. Rev.*, *21*(18–19), 2019–2046, doi:10.1016/S0277-3791(02)00009-4.

Zazo, C., J. L. Goy, C. J. Dabrio, V. Soler, C. Hillaire-Marcel, B. Ghaleb, J. A. González-Delgado, T. Bardají, and A. Cabero (2007), Quaternary marine terraces on Sal Island (Cape Verde archipelago), *Quat. Sci. Rev.*, *26*(7–8), 876–893, doi:10.1016/j.quascirev.2006.12.014.

Zazo, C., J. L. Goy, C. Hillaire-Marcel, C. J. Dabrio, J. A. González-Delgado, A. Cabero, T. Bardají, B. Ghaleb, and V. Soler (2010), Sea level changes during the last and present interglacials in Sal Island (Cape Verde archipelago), *Global Planet. Change*, *72*(4), 302–317, doi:10.1016/j.gloplacha.2010.01.006.